

Probing Nucleon Strangeness with Neutrinos : Nuclear Model Dependences

M.B. Barbaro^a, A. De Pace^a, T.W. Donnelly^b, A. Molinari^a, and M.J. Musolf^{c,d}

^a *Dipartimento di Fisica Teorica dell'Università di Torino and
Istituto Nazionale di Fisica Nucleare, Sezione di Torino,
via P.Giuria 1, I-10125 Torino, Italy*

^b *Center for Theoretical Physics,
Laboratory for Nuclear Science and Department of Physics,
Massachusetts Institute of Technology, Cambridge, MA 02139, USA*

^c *Continuous Electron Beam Accelerator Facility Theory Group, MS 12H2, Newport News,
Virginia 23606, USA*

^d *Institute for Nuclear Theory, University of Washington, Seattle, WA 98195, USA*

Abstract

The extraction of the nucleon's strangeness axial charge, Δ_s , from inclusive, quasielastic neutral current neutrino cross sections is studied within the framework of the plane-wave impulse approximation. We find that the value of Δ_s can depend significantly on the choice of nuclear model used in analyzing the quasielastic cross section. This model-dependence may be reduced by one order of magnitude when Δ_s is extracted from the ratio of total proton to neutron yields. We apply this analysis to the interpretation of low-energy neutrino cross sections and arrive at a nuclear theory uncertainty of ± 0.03 on the value of Δ_s expected to be determined from the ratio of proton and neutron yields measured by the LSND collaboration. This error compares favorably with estimates of the SU(3)-breaking uncertainty in the value of Δ_s extracted from inclusive, polarized deep-inelastic structure function measurements. We also point out several general features of the quasielastic neutral current neutrino cross section and compare them with the analogous features in inclusive, quasielastic electron scattering.

submitted to *Physical Review C*

*This work is supported in part by funds provided by the U.S. Department of Energy (D.O.E.) under contracts #DE-AC05-84ER40150, #DE-FG06-90ER40561, CEBAF and INT grants, and cooperative agreement #DE-FC02-94ER40818. M.J.M. was also supported by the National Science Foundation National Young Investigator Program.

†On leave from the Department of Physics, Old Dominion University, Norfolk, VA 23529 USA

I. INTRODUCTION

Inclusive, quasielastic (QE) weak neutral-current (NC) reactions have received considerable attention recently as a means of probing the strange quark content of the nucleon [1]. In particular, analyses of the Brookhaven experiment E734 [2–4] have generated bounds on the nucleon’s strangeness axial-vector matrix element which are essentially consistent [10] with the values for Δs , the strange-quark contribution to the nucleon spin determined from polarized deep inelastic scattering [5–9]. Less stringent bounds on the strangeness vector current form factors have also been extracted from the Brookhaven data [3,4]. In a similar vein, one expects a determination of the ratio of proton and neutron yields in the LSND experiment at Los Alamos [11] to produce even more stringent limits on some of these form factors [12,13]. The results from these studies should complement the results from several parity-violating (PV) elastic and QE electron scattering measurements currently underway at MIT-Bates [14,15] and planned for both CEBAF [16–18] and Mainz [19]. Indeed, this program of semileptonic NC scattering measurements affords one with a unique, low-energy window on the non-valence quark structure of the nucleon [1].

Since the neutrino NC reactions of interest require the detection of a final-state nucleon knocked-out of a nuclear target, a proper interpretation of the results in terms of single-nucleon physics requires that one have a sufficiently reliable understanding of the nuclear, many-body impact on the neutrino cross sections. Thus far, nuclear calculations have been performed using a relativistic Fermi Gas (RFG) model [4] and a continuum RPA approach [13]. In the present paper, we place these studies in the context of a more general framework by pointing out several features of QE neutral current scattering not previously realized in the literature. Specifically, we note the complementarity of inclusive, QE NC electron scattering, in which the outgoing electron is detected, and QE NC neutrino scattering, in which the detected particle is a nucleon. These two processes – to which we refer as t -inclusive and u -inclusive scattering, respectively – explore different regions of the two-parameter missing energy (\mathcal{E}) and missing momentum (p) space. Consequently, in the plane-wave impulse approximation (PWIA), these two types of QE NC scattering may display different sensitivities to the many-body physics which enters the one-body spectral function, $S(p, \mathcal{E})$.

We use this framework to arrive at the first (to our knowledge) published estimate of the nuclear theory uncertainty associated with the extraction of Δs from the BNL and LSND measurements. Our approach in doing so is the following. By varying the nuclear model used in analyzing the QE cross section, we change $S(p, \mathcal{E})$ and, consequently, obtain different extracted values for Δs . To be as conservative as possible, we choose two simple, tractable models lying near the extremes of the spectrum of reasonable nuclear models. Specifically, we employ the RFG model and a hybrid model (HM) involving harmonic oscillator shell model wave functions for the bound nucleons and plane waves for the continuum states. The former represents the “maximally unconfined” extreme, since it employs plane waves for bound and continuum single-particle states; additionally, as discussed below, only the on-shell electroweak current matrix elements occur [20]. The latter is “overconfined” in the sense that a harmonic oscillator basis is used, implying that the long-range behavior of the bound single-particle wave functions is gaussian rather than exponential as should be the case with finite potentials. Our approach in the present work is to model only these extremes

to explore the “worst-case scenario” for extracting Δs from QE neutrino scattering.

In fact, these two models reproduce rather well the experimental QE response for inclusive electron scattering, especially for integrated quantities such as the Coulomb sum rule [21] or the responses discussed in the present work, despite the significant differences found in the behavior of the respective spectral functions in (\mathcal{E}, p) space. We expect that the spread in extracted values of Δs obtained using more sophisticated treatments of the response, such as those which include the effects of correlations and more realistic single-particle wave functions, will be reasonably characterized by the difference between the RFG and HM values. We take as the nuclear theory error, $\delta_{\text{nuc}}(\Delta s)$, the difference between $\Delta s(\text{RFG})$ and $\Delta s(\text{HM})$. We find that at the kinematics of the LSND experiment, $\delta_{\text{nuc}}(\Delta s) \approx \pm 0.25$ when the individual proton or neutron knockout cross sections are used. This error is roughly as large in magnitude as the average value for Δs determined from the deep-inelastic measurements. If, however, one considers the ratio R_ν of proton to neutron yields rather than the individual cross sections, as has been proposed for the interpretation of the LSND data [12,13], we find that the magnitude of $\delta_{\text{nuc}}(\Delta s)$ is reduced by more than an order of magnitude. In this case, the nuclear theory uncertainty is significantly smaller than estimates of the theoretical SU(3)-breaking uncertainty in the deep inelastic values for Δs [22,23]. From this standpoint, our results complement those of Ref. [13] which analyzed the impact of final-state interactions (FSI) on the extraction of Δs from QE neutrino cross sections and which found that use of R_ν , as compared with the individual cross sections, significantly reduces one’s sensitivity to distortion in the outgoing nucleon’s wave function.

In the remainder of this paper, we discuss these features in more detail. A reader primarily interested in the application of our analysis to the extraction of Δs is encouraged to read Sections V and VI, along with Eqs. (32-35) of Sec. III. The reader interested as well in the general features of u - and t -channel QE cross sections is directed to Sec. II, where we discuss the difference between QE neutral current neutrino and electron scattering in general terms; Sec. III, in which we consider the implications of this difference for the (PWIA) analysis of QE scattering; and Sec. IV, where we specify further to the RFG. Section VII summarizes our conclusions and is followed by an Appendix.

II. INCLUSIVE t - AND u -CHANNEL SCATTERING

The leading order exclusive QE cross section is generated by the Feynman amplitude associated with the diagram of Fig. 1. Here, a lepton ℓ scatters off an A -body nucleus to a final lepton state ℓ' via the exchange of a vector boson V . In the scattering, a nucleon N is knocked out leaving behind an $(A - 1)$ -body daughter nucleus generally in an excited state. We let $K^\mu = (\epsilon, \mathbf{k})$ and $K'^\mu = (\epsilon', \mathbf{k}')$ denote the initial and final lepton momenta, respectively, $P_N^\mu = (E_N, \mathbf{p}_N)$ the four-momentum of the ejected nucleon and $-\mathbf{p}$ the three-momentum of the recoiling daughter nucleus.

Following [24] we define the missing energy \mathcal{E} as

$$\mathcal{E} \equiv \sqrt{\mathbf{p}^2 + M_{A-1}^{*2}} - \sqrt{\mathbf{p}^2 + M_{A-1}^2}, \quad (1)$$

where M_{A-1} and M_{A-1}^* are the masses of the recoiling nucleus in its ground and excited states respectively. Thus the missing energy used in this work actually corresponds to the

excitation energy of the residual nucleus in a frame where it is moving with a momentum $-\mathbf{p}$. The conditions for four-momentum conservation in the laboratory frame (target nucleus at rest) read

$$\epsilon + M_A = \epsilon' + E_N + \mathcal{E} + \sqrt{\mathbf{p}^2 + M_{A-1}^2} \quad (2a)$$

$$\mathbf{k} = \mathbf{k}' + \mathbf{p}_N - \mathbf{p} . \quad (2b)$$

If we further introduce the nucleon kinetic energy $T_N = E_N - m_N$, the nuclear recoil energy $T_{A-1} = \sqrt{\mathbf{p}^2 + M_{A-1}^2} - M_{A-1}$ and the positive nuclear separation energy $E_S = M_{A-1} + m_N - M_A$, then one may rewrite Eq. (2b) as

$$\epsilon = \epsilon' + T_N + \mathcal{E} + T_{A-1} + E_S . \quad (3)$$

At this point, we refer to Eqs. (2b) and (3) along with Fig. 1 to describe the difference between QE (e, e') N and QE (ν, N) ν' kinematics. In the former case, the initial and final lepton energies and three-momenta are fixed experimentally. Thus, one may specify a given value of the energy transfer $\omega = \epsilon - \epsilon'$ and three-momentum transfer $\mathbf{q} = \mathbf{k} - \mathbf{k}'$ by properly selecting the beam energy and momentum and the lepton detector settings. The experimentally-fixed Lorentz invariant for this process is $Q^2 = \omega^2 - \mathbf{q}^2 < 0$ and we correspondingly refer to this process as “ t -inclusive” scattering. Further, by combining Eqs. (2b) and (3), we may obtain the following relation between the missing energy and recoil momentum:

$$\mathcal{E}(\mathbf{p}) = \omega - T_{A-1} - E_S - \left[\sqrt{m_N^2 + (\mathbf{p} + \mathbf{q})^2} - m_N \right] , \quad (4)$$

where the quantity in the square brackets is just T_N . Note that T_{A-1} also carries a dependence on p^2 . However, for typical targets in QE scattering (*e. g.*, ^{12}C), T_{A-1} is much smaller than the other energies involved in the problem so that one may usually neglect it without introducing any significant error. Eq. (4) actually defines a continuous family of curves, parameterized by the angle between \mathbf{p} and \mathbf{q} . This family is accordingly bounded by the curve we denote by \mathcal{E}^- , corresponding to $\cos(\hat{p} \cdot \hat{q}) = -1$ (\mathbf{p} and \mathbf{q} anti-parallel) and the curve \mathcal{E}^+ , for which $\cos(\hat{p} \cdot \hat{q}) = 1$ (\mathbf{p} and \mathbf{q} parallel).

To get the t -inclusive cross section, one must integrate over the three-momenta of the undetected particles (daughter nucleus and outgoing nucleon). As we show below, this corresponds to integrating over the region in the (\mathcal{E}, p) space lying between the two curves \mathcal{E}^+ and \mathcal{E}^- . In fact two situations may actually occur, depending upon the sign of the vertical intercept of these curves:

$$\begin{aligned} I_t &\equiv \mathcal{E}^+(0) = \mathcal{E}^-(0) \\ &= \omega - T_{A-1} - E_S - (\sqrt{q^2 + m_N^2} - m_N) . \end{aligned} \quad (5)$$

For $I_t \leq 0$, the integration region, which we denote \mathcal{D} , will be bounded by $\mathcal{E}^-(p)$ and the p -axis (Fig. 2a), while, for $I_t \geq 0$, \mathcal{D} is bounded by $\mathcal{E}^-(p)$, $\mathcal{E}^+(p)$ and the p -axis (Fig. 2b). Note that in the figures, as an orientation, we have taken typical values for q (500 MeV/c), ω (100 and 170 MeV, respectively) and $E_S = 8$ MeV. Furthermore, we have included only the portions of the curves existing in the upper right quadrant, since both \mathcal{E} and p are by

definition non-negative. For this region, the maximum value of the missing energy occurs for [20]

$$p = p_{max} = q \frac{M_{A-1}}{M_{A-1} + m_N} \quad (6)$$

and has the value

$$\begin{aligned} \mathcal{E}(p_{max}) &\equiv \mathcal{E}_{max} \\ &= \omega - E_S - \left[\sqrt{q^2 + (M_{A-1} + m_N)^2} - (M_{A-1} + m_N) \right] \\ &\simeq \omega - E_S . \end{aligned} \quad (7)$$

For typical QE kinematics, one has $\mathcal{E}_{max} \approx 100$ MeV.

Parenthetically, we note that the region \mathcal{D} depends on the independent kinematic variables for the inclusive process. For example, when the cross section for an outgoing electron of a specified energy and scattering angle is considered, one has $\mathcal{D} = \mathcal{D}(\epsilon', \theta_e)$. When the energy- or angle-integrated cross section is of interest, the region \mathcal{D} consists of the union of all regions $\mathcal{D}(\epsilon', \theta_e)$ allowed by the kinematics.

In the case of QE NC neutrino scattering, the final lepton is undetected and the four-momentum of the outgoing nucleon is specified ¹. Thus, the experimentally-fixed variables become

$$u_0 = \epsilon - E_N \quad (8a)$$

$$\mathbf{u} = \mathbf{k} - \mathbf{p}_N . \quad (8b)$$

The corresponding Lorentz invariant in this case is $U^2 = u_0^2 - |\mathbf{u}|^2$ and we refer to this process as “ u -inclusive” scattering. From the conservation relations (Eqs. (2b) and (2b)), one has

$$u_0 = \mathcal{E} + \epsilon' + T_{A-1} + E_S - m_N \quad (9a)$$

$$\mathbf{u} = \mathbf{k}' - \mathbf{p} . \quad (9b)$$

Since the neutrino is massless, one has that $\epsilon' = |\mathbf{k}'| = |\mathbf{u} + \mathbf{p}|$, so that Eq. (9b) may be re-written as

$$\mathcal{E}(p) = u_0 - E_S + m_N - T_{A-1} - |\mathbf{u} + \mathbf{p}| . \quad (10)$$

Eq. (10) is the u -channel analog of the relation in Eq. (4). Neglecting the small p^2 -dependent recoil kinetic energy and defining a quantity δ as

$$\delta \equiv u_0 - E_S + m_N , \quad (11)$$

we obtain the following boundaries for the region \mathcal{D} over which one should integrate to get the u -inclusive cross section

¹ In practice, detectors include the full solid angle for the outgoing nucleon.

$$\mathcal{E}^+ = \delta - (u + p), \quad \mathbf{u} \text{ and } \mathbf{p} \text{ parallel} \quad (12a)$$

$$\mathcal{E}^- = \delta - |u - p| = \begin{cases} \mathcal{E}_>^- = \delta - (u - p) & \mathbf{u} \text{ and } \mathbf{p} \text{ anti-parallel, } u > p \\ \mathcal{E}_<^- = \delta - (p - u) & \mathbf{u} \text{ and } \mathbf{p} \text{ anti-parallel, } u < p \end{cases} \quad (12b)$$

We note that the reason for the appearance of two cases for \mathcal{E}^- is that the undetected particle in this instance is massless. Consequently, ϵ' – and therefore \mathcal{E} – depends linearly on $|\mathbf{u} + \mathbf{p}|$. In the t -channel case, the un-detected outgoing particle is massive, rendering the dependence of \mathcal{E} on $|\mathbf{q} + \mathbf{p}|$ quadratic and the relative magnitudes of q and p inconsequential.

To assess the extent and the shape of the region \mathcal{D} it helps to observe that in the u -inclusive scattering the maximum of the curve \mathcal{E}^- occurs for

$$p = p_{max} = u \quad (13)$$

where $\mathcal{E}^-(p)$ assumes the value

$$\mathcal{E}^-(p_{max}) = \delta . \quad (14)$$

The relations in Eqs. (13) and (14) are the u -channel versions of Eqs. (6) and (7). In both cases, the location of the maximum depends linearly on the magnitude of the independent vector quantity (q or u) while the height of the maximum is linear in the independent time-like quantity (ω or u_0).

For future reference, we specify the two values of the momentum ($p_{<}^-$ and $p_{>}^-$) where \mathcal{E}^- vanishes. They are given by

$$p_{<}^- = u - \delta \quad \text{and} \quad p_{>}^- = u + \delta , \quad (15)$$

$p_{>}^-$ being positive definite whereas $p_{<}^-$ can be either positive or negative. On the other hand $\mathcal{E}^+(p)$ vanishes for

$$p^+ = \delta - u , \quad (16)$$

which can be positive or negative.

Again in complete analogy with the t -channel the curves $\mathcal{E}^-(p)$ and $\mathcal{E}^+(p)$ intercept each other at $p = 0$, where their common value is

$$I_u \equiv \mathcal{E}^-(0) = \mathcal{E}^+(0) = \delta - u . \quad (17)$$

Let us denote by $\mathcal{D}(\theta_N)$ the allowed region in the (\mathcal{E}, p) plane at fixed θ_N , the angle between \mathbf{k} and \mathbf{p}_N .² Two situations can then occur corresponding to two different shapes for this region: Either I_u is positive or is negative. In the latter case $p_{<}^-$ is positive and $\mathcal{D}(\theta_N)$ is a triangle, lying of course in the physical quadrant of the (\mathcal{E}, p) plane. The area of the triangle is δ^2 ; hence, it is fixed once the moduli of the momenta of the incoming neutrino

²As in the t -channel case, the integration region depends on the two independent kinematic variables. In the present context, it is useful to choose one of them to be θ_N and to suppress the dependence of \mathcal{D} on the other.

and outgoing nucleon are given. On the other hand the *position* of the triangle in the (\mathcal{E}, p) plane depends on θ_N , as well as on $k = |\mathbf{k}|$ and $p_N = |\mathbf{p}_N|$ (indeed, according to Eq. (13), the upper vertex of the triangle is fixed by u , whose value also depends on these variables (see Eq. (8b))).

This situation is illustrated in Fig. 3a for kinematics typical of the LSND experiment, namely by choosing $\epsilon = 200$ MeV and $T_N = 60$ MeV ($p_N = 341$ MeV/c). We thus see that when \mathbf{p}_N and \mathbf{k} are antiparallel ($\theta_N = 180^\circ$), I_u is indeed negative and \mathcal{D} is given by the triangle on the right-hand side of the figure.

As θ_N is varied from antiparallel (180°) to parallel (0°) while keeping k and p_N fixed the value of u decreases and the triangle moves continuously in the leftward direction. When I_u is positive, then $\mathcal{D}(\theta_N)$ becomes quadrangular, as displayed in Fig. 3b for the case in which \mathbf{k} and \mathbf{p}_N are parallel and for kinematics typical of the BNL experiment. The area of the quadrangle is given by $2u\delta - u^2$.

For an experimental situation in which nucleons are detected over the full 4π solid angle (as in LSND), the global integration region \mathcal{D} will be given by taking the union of sub-regions $\mathcal{D}(\theta_N)$ for all θ_N . For example, as illustrated in the two panels of Fig. 3 for cases with $I_u < 0$ and $I_u > 0$, respectively, the regions \mathcal{D} are defined by the lines whose vertices are labeled $ABCD$ ($I_u < 0$: quadrangle) and $ABCDE$ ($I_u > 0$: pentagon), respectively.

III. PLANE-WAVE IMPULSE APPROXIMATION

Much of the interest in the inclusive $(e, e')N$ and $(\nu, N)\nu'$ scattering reactions stems from an interpretation of the cross sections employing the PWIA. Invoking the PWIA corresponds to modeling the shaded vertex in Fig. 1 as illustrated in Fig. 4. Here, one assumes that only one nucleon participates in the scattering by absorbing the virtual vector boson V , the remainder of the nucleus acting just as a spectator. Three-momentum conservation in the laboratory system requires that the struck nucleon has momentum \mathbf{p} since the initial nucleus is at rest and the daughter nucleus recoils with momentum $\mathbf{p}_{A-1} = -\mathbf{p}$. Before absorbing the V , the struck nucleon has energy E and in general does not lie on the mass-shell. In the limit that final-state interactions are neglected, as is indeed the case in the PWIA, the outgoing nucleon is assumed to be on the mass-shell with an energy $E_N = \sqrt{\mathbf{p}_N^2 + m_N^2}$. Under these assumptions, the differential cross section can be written in terms of kinematic and phase space factors, the square of the invariant amplitude for scattering of the incident lepton from a single nucleon — half-off-shell, since the struck nucleon is in general off-shell [25] — and a function $S(p, \mathcal{E})$, referred to as the spectral function, which carries information on the probability of finding a nucleon inside the nucleus with momentum \mathbf{p} and energy

$$E = M_A - \sqrt{\mathbf{p}^2 + M_{A-1}^2} - \mathcal{E} , \quad (18)$$

It reads:

$$d\sigma = \frac{1}{4kM_A} |\overline{\mathcal{M}}|^2 \frac{d^3k'}{(2\pi)^3 2\epsilon'} \frac{d^3p_N}{(2\pi)^3 2E_N} \frac{d^3p_{A-1}}{(2\pi)^3 2E_{A-1}^*} \\ \times (2\pi)^4 \delta^{(4)}(K + P_A - K' - P_N - P_{A-1}) \quad (19)$$

where $P_A^\mu = (M_A, \mathbf{0})$ is the four-momentum of the target nucleus, $P_{A-1}^\mu = (E_{A-1}, -\mathbf{p})$ is the four-momentum of the daughter nucleus, \mathcal{M} is the invariant lepton-nucleus scattering amplitude, and where the bar over \mathcal{M} denotes the appropriate average over initial spins and sum over final spins. Performing the integral over \mathbf{p}_{A-1} gives

$$d\sigma = \frac{1}{4kM_A} \overline{|\mathcal{M}|^2} \frac{d^3k'}{(2\pi)^3 2\epsilon'} \frac{d^3p_N}{(2\pi)^3 2E_N} \frac{2\pi}{2E_{A-1}^*} \times \delta(\epsilon + M_A - \epsilon' - E_N - E_{A-1}^*) . \quad (20)$$

The general form for the square of the invariant amplitude is

$$\overline{|\mathcal{M}|^2} = g^4 D_V(Q^2)^2 L_{\mu\nu} W^{\mu\nu} , \quad (21)$$

where g is the strength of the fermion-vector boson coupling, $D_V(Q^2) = (Q^2 - M_V^2 + i\epsilon)^{-1}$, M_V is the electroweak vector boson mass, $L_{\mu\nu}$ is the usual leptonic tensor appearing in semi-leptonic scattering and $W_{\mu\nu}$ is the corresponding hadronic tensor. They are given by the following well-known expressions:

$$L_{\mu\nu} = \frac{1}{8} \text{Tr} [\bar{u}(k', s') \Gamma_\mu u(k, s) \bar{u}(k', s') \Gamma_\nu u(k, s)] \quad (22a)$$

$$W_{\mu\nu} = \langle A | \hat{J}_\mu^\dagger | f \rangle \langle f | \hat{J}_\nu | A \rangle , \quad (22b)$$

where $|A\rangle$ is the initial target nucleus, $|f\rangle$ is the final hadronic state, Γ_μ is a Lorentz structure associated with the lepton-vector boson vertex, \hat{J}_λ is the hadronic current operator, and where the appropriate average over initial and sum over final hadronic states is understood in Eqs. (20)-(22b). Furthermore, in Eq. (22b) the spinors are normalized according to the Bjorken and Drell conventions [26] and the weak vertices are given by the usual expressions.

In the PWIA framework only the one-body component of the nucleonic current, namely

$$\hat{J}_\lambda = \sum_{s,s'} \int \frac{d^3k}{(2\pi)^3} \int \frac{d^3k'}{(2\pi)^3} \frac{1}{2E_k} \frac{1}{2E_{k'}} (2\pi)^3 \delta(\mathbf{k}' - \mathbf{k} - \mathbf{q}) \times \bar{u}_N(k', s') \Gamma_\lambda^N u(k, s) \hat{a}^\dagger(k', s') \hat{a}(k, s) , \quad (23)$$

is kept. In the above $\hat{a}^\dagger(k, s)$ and $\hat{a}(k, s)$ are, respectively, the operators that create and annihilate bound nucleons (*i.e.*, in momentum space, having Fourier component k and spin projection s) and Γ_λ^N is the Lorentz structure associated with the single-nucleon current matrix element [25]. Normalizing the states according to Ref. [26],

$$\langle \mathbf{p} | \mathbf{q} \rangle = (2\pi)^3 2E_p \delta(\mathbf{p} - \mathbf{u}) , \quad (24)$$

and substituting the expression in Eq. (23) into Eq. (22b) yields

$$W_{\mu\nu} = \sum_{s,s'} \left(\frac{1}{2E_p} \right)^2 \langle A | \hat{a}^\dagger(p, s) | A-1 \rangle \langle A-1 | \hat{a}(p, s) | A \rangle \times w_{\mu\nu}(\mathbf{p}, \mathbf{p}_N) , \quad (25)$$

where

$$w_{\mu\nu}(\mathbf{p}, \mathbf{p}_N) = \bar{u}(p, s)\Gamma_\mu u(p_N, s')\bar{u}(p_N, s')\Gamma_\nu u(p, s) \quad (26)$$

is the so-called single-nucleon tensor and the ket $|A - 1\rangle$ represents the daughter nucleus in either its ground state or one of its excited states. The replacement of E_{A-1} with $\mathcal{H} \equiv \hat{H} - E_{A-1}^{(0)}$ inside the δ -function appearing in Eq. (20) allows one to perform a sum over all daughter-nucleus states by making use of the closure relation. One then obtains

$$\begin{aligned} d\sigma &= \frac{1}{4kM_A}(2\pi) \left(\frac{1}{2E}\right)^2 g^4 D_V(Q^2)^2 L_{\mu\nu} \sum_{s,s'} w^{\mu\nu}(\mathbf{p}, \mathbf{p}_N) \\ &\times \langle A | \hat{a}^\dagger(p, s) \delta(\epsilon + M_A - \epsilon' - E_N - E_{A-1}^0 - \hat{\mathcal{H}}) \hat{a}(p, s) | A \rangle \frac{d^3 k'}{(2\pi)^3 2\epsilon'} \frac{d^3 p_N}{(2\pi)^3 2E_N} . \end{aligned} \quad (27)$$

Noticing that $E = E_N - \epsilon + \epsilon'$ and defining the chemical potential $\mu \equiv M_A - E_{A-1}^0$ (not to be confused with a Lorentz index), one has

$$\begin{aligned} d\sigma &= \frac{(2\pi)^4}{2k} \left(\frac{1}{2E}\right) g^4 D_V(Q^2)^2 L_{\mu\nu} w^{\mu\nu}(\mathbf{p}, \mathbf{p}_N) \\ &\times S(p, \mathcal{E}) \frac{d^3 k'}{(2\pi)^3 2\epsilon'} \frac{d^3 p_N}{(2\pi)^3 2E_N} , \end{aligned} \quad (28)$$

where the spectral function is

$$\begin{aligned} S(p, \mathcal{E}) &= \frac{1}{(2\pi)^3} \left(\frac{1}{2E}\right) \left(\frac{1}{2M_A}\right) \\ &\times \langle A | \hat{a}^\dagger(p, s) \delta(E + \hat{\mathcal{H}} - \mu) \hat{a}(p, s) | A \rangle . \end{aligned} \quad (29)$$

A further elementary elaboration of Eq. (28) leads to the exclusive cross section

$$\begin{aligned} \frac{d^4\sigma}{d\Omega' dk' d\Omega_N dE_N} &= \frac{1}{(2\pi)^2} \frac{1}{2k} \frac{1}{2E} g^4 D_V(Q^2)^2 \\ &\times L_{\mu\nu} w^{\mu\nu}(\mathbf{p}, \mathbf{p}_N) S(p, \mathcal{E}) \frac{k'}{2} \frac{p_N}{2} . \end{aligned} \quad (30)$$

From Eq. (28) or (30) one obtains the t -channel (u -channel) inclusive cross section by integrating over the undetected nucleon (lepton) momentum. In so-doing, it is convenient to convert to integrals over the variables p and \mathcal{E} . To this end, we first make use of the fact that $\mathbf{p}_N = \mathbf{q} + \mathbf{p}$ and $\mathbf{k}' = \mathbf{u} + \mathbf{p}$, so that for fixed \mathbf{q} one has $d^3 p_N = d^3 p$ and for fixed \mathbf{u} one has $d^3 k' = d^3 p$. Second, we write $d^3 p = d\phi d\cos\theta p^2 dp$, where (θ, ϕ) are defined with respect to \mathbf{q} in the case of t -channel scattering and with respect to \mathbf{u} in the case of u -channel scattering. Third, we make use of the $(\mathcal{E}, \mathbf{p})$ relations in Eqs. (3) and (7) to transform from $d\cos\theta$ to $d\mathcal{E}$, getting

$$d\cos\theta = \begin{cases} (E_N/pq)d\mathcal{E} , & t\text{-channel} \\ (\epsilon'/pu)d\mathcal{E} , & u\text{-channel} \end{cases} \quad (31)$$

respectively. Finally, we obtain for the cross section

$$d\sigma = (2\pi) \int_{\mathcal{D}} d\phi \int pdp \int d\mathcal{E} S(p, \mathcal{E}) \left(\frac{1}{16\epsilon E} \right) g^4 D_V(Q^2)^2 \times L_{\mu\nu} w(\mathbf{p}, \mathbf{p}_N)^{\mu\nu} \frac{dQ_f}{\rho}, \quad (32)$$

where

$$\frac{dQ_f}{\rho} = \frac{1}{q} \frac{d^3 k'}{(2\pi)^3 2\epsilon'}, \quad t\text{-channel} \quad (33a)$$

$$\frac{dQ_f}{\rho} = \frac{1}{u} \frac{d^3 p_N}{(2\pi)^3 2E_N}, \quad u\text{-channel}, \quad (33b)$$

\mathcal{D} denoting the allowed region of integration in the (\mathcal{E}, p) plane (for the case of electrons, we have assumed the extreme relativistic limit ($k = \epsilon$)).

From the above, the explicit expressions

$$\frac{d^2\sigma}{d\Omega' d\epsilon'} = \frac{1}{2\pi} \frac{1}{32} \frac{k'}{\epsilon} \frac{1}{q} g^4 D_V(Q^2)^2 \times \int_{\mathcal{D}} pdp \int \frac{d\mathcal{E}}{E} S(p, \mathcal{E}) \overline{L_{\mu\nu} w^{\mu\nu}(\mathbf{p}, \mathbf{p}_N)} \quad (34)$$

and

$$\frac{d^2\sigma}{d\Omega_N dE_N} = \frac{1}{2\pi} \frac{1}{32} \frac{p_N}{\epsilon} \frac{1}{u} g^4 \times \int_{\mathcal{D}} pdp \int \frac{d\mathcal{E}}{E} S(p, \mathcal{E}) \overline{L_{\mu\nu} w^{\mu\nu}(\mathbf{p}, \mathbf{p}_N)} D_V(Q^2)^2 \quad (35)$$

for the t - and u -inclusive cross sections, respectively, follow. Note that the azimuthal integration has already been carried out, introducing an azimuthally averaged single-nucleon tensor (or, equivalently, single-nucleon cross section) as done, for example, in Refs. [24,20].

The formula given in Eq. (34) constitutes the conventional starting point for the analysis of inclusive QE (e, e') scattering in the PWIA.³ Previously reported treatments of QE (ν, N) scattering, however, have not made use of this framework [13,4]. The advantage of writing $d\sigma(\nu, N)$ in the form of Eq. (32) is two-fold: First, it makes explicit the dependence of the QE cross section on the experimentally-fixed kinematic variables (u_0, \mathbf{u}) via the specification of the integration region \mathcal{D} and the appearance of u in the integration measure $1/\rho$. Second, it makes the role of the one-body nuclear spectral function explicit, thereby making the nuclear model-dependence of the cross section more transparent.

When the single-nucleon tensor $w^{\mu\nu}(\mathbf{p}, \mathbf{p}_N)$ refers to an on-shell nucleon, the expressions in Eqs. (32) and (34) carry a dependence on the free-nucleon form factors. For general neutral current scattering, three such form factors contribute: $G_i(Q^2)$, where $i = E, M$, or A denotes the Sachs electric and magnetic form factors and the axial-vector form factor, respectively [1]. In the case of t -channel scattering, one is then able to employ Eq. (32) to

³Typically, one sees integrations over E rather than \mathcal{E} in the literature.

extract information on the single-nucleon form factors at a single value of Q^2 . Since t is fixed experimentally in this case, one may factor the form factors out of the integral over (\mathcal{E}, p, ϕ) , leaving only an integral over the spectral function and various kinematic factors resulting from the contraction of $L_{\mu\nu}$ and $w^{\mu\nu}$. To the extent that one's choice of $S(p, \mathcal{E})$ is realistic and that the PWIA is valid, one obtains a more or less reliable determination of the $G_i(Q^2)$. An important feature of t -channel scattering is that q , ω and the electron scattering angle θ_e can all be fixed in an inclusive measurement, allowing (in the plane-wave Born approximation) the various longitudinal (L), transverse (T), \dots hadronic responses to be separated before attempting to determine the $G_i(Q^2)$, to be contrasted with the situation discussed below for u -channel inclusive scattering.

In contrast, even were the on-shell approximation to be a good one, u -channel neutrino scattering does not allow one to extract the G_i at a single value of Q^2 . Since U^2 rather than Q^2 is fixed, the value of Q^2 varies as one integrates over the allowed region in (\mathcal{E}, p) space. For example, for kinematics typical of the LSND experiment (see Fig. 3), Q^2 varies over the range (see next Section) $0 \leq |Q^2| \leq 0.06$ (GeV/c) 2 as \mathcal{E} and p vary over the allowed region \mathcal{D} (allowing the neutrino scattering angle to vary over all possible values). Similarly, for kinematics typical of the BNL experiment [2], $\epsilon = 1.3$ GeV and, say, $T_N = 500$ MeV, the corresponding range is $0 \leq |Q^2| \leq 2.3$ (GeV/c) 2 . In either case, the form factors associated with the struck nucleon contribute to the u -channel cross section over a range of Q^2 . In order to extract information about the form factors from this cross section, one is forced to adopt some parameterization for the Q^2 -dependence of the form factor and fit the parameters to the measured cross section. Furthermore, as alluded to above, in u -channel inclusive scattering the values of q , ω and the neutrino scattering angle θ_ν all vary when performing the integrations and thus no separation into isolated L, T, \dots hadronic responses is possible.

All of these aspects of u -channel inclusive scattering stand in contrast with the t -channel situation discussed above in which a parameterization-independent form factor determination is possible. Only in the case of elastic scattering from $A = 1$ targets are u - and t -channel processes equivalent. In the latter case, one has

$$(K + P_A)^2 + Q^2 + U^2 = 2m_N^2 + 2m_\ell^2 \quad , \quad (36)$$

where m_ℓ is the mass of the lepton and $(K + P_A)^2 = (\epsilon + m_N)^2 - \mathbf{k}^2 \approx m_N^2 - 2\epsilon m_N$ in the lab frame. For scattering from a single-nucleon target, then, specifying U^2 is equivalent to specifying Q^2 . Consequently, u -channel scattering can be used to perform a parametrization-independent form factor determination in this case.

Finally, as discussed in Sec. V and the Appendix, another issue to be confronted is the fact that in general the struck nucleon is initially off-shell and accordingly the relationship to on-shell single-nucleon form factors is not obvious. In the present work we use a generalization of the popular $cc1$ prescription of de Forest [25] when modeling this type of behaviour. At least within the context of this approach we shall see that this model dependence is rather weak for the observables of interest (see Sec. VI).

IV. RFG PREDICTIONS FOR u -INCLUSIVE SCATTERING

Although already considered in Ref. [4], we wish to revisit in this Section the RFG predictions for the u -inclusive scattering partly to complement the findings of that work, which are rederived here via the alternative route of integrating in proper regions of the (\mathcal{E}, p) plane, and partly to establish analytic expressions for some general features of the RFG u -inclusive cross section not presently available in the literature to our knowledge.

As discussed briefly in the previous Section, while in the t -channel it turns out to be possible to obtain a compact, simple expression for the RFG inclusive cross sections or, equivalently, for the longitudinal R_L and the transverse R_T response functions, this is not so in the u -channel. The reason is precisely the one mentioned at the end of the previous Section, namely, the Q^2 -dependence arising from the presence of the single-nucleon form factors. For the t -inclusive case, Q^2 is fixed so that the nucleon form factors may be factored out of the integrals over \mathcal{E} and p . By contrast in the u -channel Q^2 varies over the integration region \mathcal{D} ; hence the nucleon's form factors cannot be brought out of the integrals except (and then only approximately) in special kinematic situations where the $G_i(Q^2)$ vary gently over \mathcal{D} .

To provide an appreciation for the behavior of Q^2 in the (\mathcal{E}, p) plane we display its variation in Fig. 5 for the same kinematical situation of Fig. 3, considering, as an example, the instance of \mathbf{p}_N and \mathbf{k} being parallel. The explicit dependence upon \mathcal{E} and p of Q^2 turns out to be

$$Q^2 = (T_N + E_S + \mathcal{E})^2 + \frac{k}{|k \mp p_N|} \left[(k - T_N - E_S - \mathcal{E})^2 + (k \mp p_N)^2 - p^2 \right] \quad (37)$$

where the upper (lower) sign corresponds to \mathbf{k} and \mathbf{p}_N being parallel (anti-parallel). From Fig. 5, it clearly appears that Q^2 varies rapidly with p but only mildly with \mathcal{E} .

Notwithstanding this feature we try to express analytically a few general properties of the RFG u -inclusive cross section. To this end, we recall [20] that the RFG spectral function reads

$$S_{RFG}(p, \mathcal{E}) = 2\theta(k_F - p) \times \delta \left(\mathcal{E} - \sqrt{k_F^2 + m_N^2} + \sqrt{p^2 + m_N^2} \right), \quad (38)$$

where the factor 2 accounts for the spin degeneracy. Note that the above cannot be directly derived from the expression in Eq. (29), where the states are normalized according to (24). Instead, one requires the normalization

$$\langle \mathbf{p} | \mathbf{q} \rangle = 2E_p \Omega \delta_{\mathbf{k}, \mathbf{p}}, \quad (39)$$

Ω being the (large) volume enclosing the Fermi gas. Clearly, the support in Eq. (38) in the (\mathcal{E}, p) plane is nonzero only along the curve

$$\mathcal{E}^{RFG} = \sqrt{k_F^2 + m_N^2} - \sqrt{p^2 + m_N^2}. \quad (40)$$

It is then natural to expect the maximum of the u -inclusive cross section to correspond to the situation where \mathcal{D} encompasses the whole of the RFG spectral function. In the strict RFG model this requires

$$I_u = \sqrt{k_F^2 + m_N^2} - m_N = \epsilon_F - m_N = T_F > 0 , \quad (41)$$

which insures that the piece of the boundaries of \mathcal{D} stemming from \mathcal{E}^+ does not cut off a section of the curve defined by Eq. (40).

For kinematic conditions under which the $G_i(Q^2)$ vary mildly over the integration region \mathcal{D} and over variations in (u_0, \mathbf{u}) , it follows from Eq. (41) that the maximum of the cross section will occur for the following kinetic energy of the outgoing nucleon:

$$T_N^{max} = \frac{k \cos^2 \theta_N}{1 + m_N/(2k) + k/(2m_N) \sin^2 \theta_N} . \quad (42)$$

For purposes of comparison, we note that the same principle of maximum overlap between the support of the spectral function and \mathcal{D} leads to the following result for the maximum of the cross section:

$$\begin{aligned} \omega_{max} &= \sqrt{\mathbf{q}^2 + m_N^2} - m_N \Rightarrow \\ \omega_{max} &= |Q_{max}^2|/2m_N \equiv [q^2 - \omega_{max}^2]/2m_N , \end{aligned} \quad (43)$$

in the t -channel (see Ref. [20]). Actually Eq. (43) holds exactly for properly reduced RFG response functions where the single-nucleon form factor dependences are removed (see Ref. [27]). If not so reduced, then at high momentum transfer the prediction in Eq. (43) is appreciably altered by the single-nucleon physics. For the u -channel case, we find that the expression in Eq. (42), which provides the maximum for the cross section, is valid only for large k and small θ_N , where it turns out that the single-nucleon physics has less of an impact.

A novel feature of the RFG u -inclusive cross section, with respect to the t -inclusive one, is its unexpected vanishing in some range of T_N . To illustrate this feature, we recall that the u -inclusive cross section is fixed by three parameters: k , p_N and θ_N . Now for $p_N^- = u - \delta > k_F$ no overlap exists between \mathcal{D} and the curve of Eq. (40): Hence the vanishing of the cross section. This situation clearly corresponds to a negative value of the intercept I_u . However, when the intercept I_u is positive, the cross section might also vanish, provided that $\delta - u$ is larger than k_F . One is thus led to consider the equation

$$u - \delta = k_F , \quad (44)$$

which admits two real, positive roots, namely

$$T_N^{(1,2)} = \frac{2m_n k^2 \cos^2 \theta_N - \alpha(2k - \alpha)(k + m_N - \alpha) \pm k |\cos \theta_N| \sqrt{\Delta}}{2(k + m_N - \alpha + k \cos \theta_N)(k + m_N - \alpha - k \cos \theta_N)} \quad (45)$$

with

$$\begin{aligned} \Delta &= 4m_n^2 k^2 \cos^2 \theta_N \\ &\quad - \alpha(2k - \alpha)(2m_N - \alpha)(2k + 2m_N - \alpha) \end{aligned} \quad (46)$$

if, and only if,

$$\cos \theta_N \geq \frac{\sqrt{\alpha(2m_N - \alpha)(2k - \alpha)(2k - \alpha + 2m_N)}}{2m_N k}, \quad (47)$$

where $\alpha = E_S + k_F$ and

$$E_S = m_N - \sqrt{k_F^2 + m_N^2} \approx -\frac{k_F^2}{2m_N} \quad (48)$$

is the *negative* separation energy of the RFG (see Ref. [20]).

It thus appears that a critical angle, θ_0 , exists such that for $\theta_N \leq \theta_0$ the u -inclusive cross section vanishes in the range $T_N^{(1)} \leq T_N \leq T_N^{(2)}$. The asymptotic value of θ_0 for large lepton momenta k is 52° at $k_F = 225$ MeV/c and θ_0 exists only for $k \geq k_F$. Note that when $k = k_F$ then $\theta_N = 0^\circ$ and the two roots in Eq. (45) coincide, namely

$$T_N^{(1)} = T_N^{(2)} = -E_S. \quad (49)$$

For $k > k_F$ the maximum distance between the roots in Eq. (45) (the maximum range over which the cross section vanishes) occurs for $\theta_N = 0$. Then it gradually decreases as θ_N is increased from 0° to θ_0 .

A final consideration relates to the traditional handling of Pauli blocking in the RFG. In the t -channel, this blocking gives rise to the experimentally unsupported linear energy behaviour of the cross section at low ω when $q < 2k_F$. Consequently, one does not expect the RFG cross section to be credible until $q > 2k_F$. In the u -channel, Pauli correlations may also be incorporated, although one may debate the appropriate method for treating them. At the crudest level of approximation, for example, one may model these correlations simply by requiring that the cross section vanish for $p_N < k_F$ ($T_N < T_F$). Importantly for comparisons with the LSND measurements, an experimental cut is made at $T_N = 60$ MeV ($p_N \approx 340$ MeV), lessening the impact of such modeling.

Let us now conclude this Section by presenting some typical u -inclusive neutrino cross sections using the RFG. For this purpose we first recall that the RFG is a symmetric system with equal number of protons and neutrons ($Z=N=A/2$), all of them on the mass-shell. Then we insert the spectral function of Eq. (38) into Eq. (35), yielding

$$\begin{aligned} \frac{d^2\sigma}{d\Omega_N dE_N} &= \mathcal{N} \frac{1}{\rho} \frac{1}{(2\pi)^4} \frac{1}{16} \frac{p_N}{u} \left(\frac{g}{M_V} \right)^4 \\ &\times \int_{\mathcal{D}} dp p \int d\mathcal{E} \frac{S_{RFG}(p, \mathcal{E})}{E} L_{\mu\nu} w^{\mu\nu}(\mathbf{p}, \mathbf{p}_N) \end{aligned} \quad (50)$$

where $\rho = 2k_F^3/(3\pi^2)$ is the Fermi gas density and \mathcal{N} indicates either the proton (Z) or the neutron (N) number. Furthermore, when applied to neutrino scattering, the coupling to mass ratio which enters is $g/(4 \cos \theta_W M_W) = \sqrt{G_F}/(2\sqrt{2})$, G_F being the Fermi constant (we have assumed the ρ parameter to be equal to unity for simplicity), and [4]

$$L_{\mu\nu} w^{\mu\nu}(\mathbf{p}, \mathbf{p}_N) = 2[V_{VV} + V_{VA} + V_{AA}], \quad (51)$$

where explicit expressions both for the on- and off-shell quantities in Eq. (51) are given in terms of the weak neutral current form factors in the Appendix.

Since our focus in this work is on ^{12}C , we take $k_F = 225 \text{ MeV}/c$. The results of our calculations are displayed in Fig. 6a, where we again consider kinematics typical of the LSND experiment ($\epsilon = 200 \text{ MeV}$) and, for purposes of illustration, we explore two different orientations between the incoming neutrino and the outgoing nucleon (either proton or neutron), namely $\theta_N = 20^\circ$ and 60° . We observe the following:

- i) the cross section decreases with the angle θ_N for low values of k , at least for not too large values of θ_N ;
- ii) the neutron cross section is larger than the proton cross section.

In Fig. 7a the neutrino cross sections for the RFG (but with only outgoing protons) are calculated using kinematics corresponding to the average energy of the Brookhaven neutrinos ($\epsilon = 1.3 \text{ GeV}$). In this case, the experimental cut is made at $T_N = 200 \text{ MeV}$ and so Pauli blocking plays a minor role. In contrast to the situation for low-energy neutrinos, the cross sections increase with θ_N . In addition, the previously noted possibility of a vanishing u -inclusive cross section for certain values of θ_N appears in Fig. 7a: A sizable gap in the cross section occurs for $\theta_N = 20^\circ$, but not for $\theta_N = 60^\circ$, since the value of the limiting angle in this case turns out to be $\theta_0 = 25.7^\circ$.

V. HM PREDICTIONS FOR u -INCLUSIVE SCATTERING

We next turn to the hybrid harmonic oscillator shell model [20] and its extensions to inclusion of a spreading width. While these choices clearly do not exhaust the list of possibilities — in particular in this work we do not deal with the final-state dynamics issues that were treated in Ref. [13] — we are able to set a scale for the theoretical uncertainty in the extracted value of $G_A^{(s)}$, as discussed in the next Section.

The HM developed in Ref. [20] differs from the RFG in that it has the states below the Fermi surface confined, therefore requiring the struck nucleon to be off-shell (see the Appendix). In the PWIA the states above the Fermi surface are taken to be plane waves. Accordingly in this model one accounts for the confinement of the nucleons in the initial state, which is of course important for a realistic description of low-energy neutrino-nucleus inelastic scattering, however at the expense of losing the Lorentz covariance characteristic of the RFG. In other words the hybrid model is only semi-relativistic.

In principle, this confinement is generated by a Hartree-Fock well; in practice, as a simple, tractable model we use a harmonic oscillator as the confining potential, namely

$$V(r) = \frac{1}{2}m_N\omega_0^2r^2 - \bar{V} , \quad (52)$$

\bar{V} being a positive quantity fixed in such a way to reproduce the experimental separation energies, $E_s = 15.96$ (18.72) MeV for protons (neutrons). For the oscillator frequency, we use $\omega_0 = 41/A^{1/3} \text{ MeV}$. The HM spectral function is then easily found to be

$$\begin{aligned}
S^{HM}(p, \mathcal{E}) &= \sum_{N=0}^{N_{MAX}} \delta[\mathcal{E} - (N_{MAX} - N)\omega_0 + \Delta E] n_N(p) \\
&= \sum_{N=0}^{N_{MAX}} \delta[E - (N + \frac{3}{2})\omega_0 - \bar{V} - m_N] n_N(p)
\end{aligned} \tag{53}$$

where the shift in the excitation energy \mathcal{E} stemming from the binding of the nucleons is denoted by ΔE . In the above, the momentum distribution for a given shell identified by the quantum number $N = 2n + \ell$ is given by

$$n_N(p) = 2 \sum_{n\ell} \frac{2\ell + 1}{4\pi} |\varphi_{n\ell}(p)|^2, \tag{54}$$

where $\varphi_{n\ell}(p)$ are the harmonic oscillator radial wave functions in momentum space. For simplicity (and in good accord, for example, with mean-field descriptions of light $N = Z$ nuclei) we assume the momentum distributions of protons and neutrons in a given shell to be the same. In contrast with the RFG spectral function discussed above one finds that the HM spectral function in Eq. (53) is nonzero on a set of parallel lines in the (\mathcal{E}, p) plane, one for each shell (*e. g.*, two lines for ^{12}C), at variance with the case of the RFG, whose spectral function is nonzero on the single curve given by Eq. (40). As mentioned in the Introduction, in the present work when considering the HM we employ only a harmonic oscillator basis with its overly strong confinement to provide the strongest contrast with the RFG model — a sort of “worst-case” scenario.

As one straightforward extension of the above formalism where specific classes of correlations effects may be modeled we also allow the single-particle states to acquire a spreading width. This extension is implemented by adding a complex self-energy to the single-particle energies, thus defining the fermion propagator as

$$G_{HM}^{(SW)}(p, E) = \sum_{N=0}^{N_{MAX}} \frac{n_N(p)}{E - [\epsilon_N + \Sigma(\epsilon_N) - \epsilon_F]}, \tag{55}$$

where $\epsilon_N = m_N + (N + \frac{3}{2})\omega_0 - \bar{V}$ represents the energy of the nucleon in the N th shell. The self-energy Σ , of course, arises from second- (or higher-) order insertions on the fermion propagation lines: Here, we adopt the point of view of parametrizing it in terms of the following function

$$\Sigma(\epsilon) = \Delta(\epsilon) - i \frac{\gamma(\epsilon)}{2}, \tag{56}$$

with

$$\gamma(\epsilon) = 2\alpha \frac{\epsilon^2}{\epsilon^2 + \epsilon_0^2} \frac{\epsilon_1^2}{\epsilon^2 + \epsilon_1^2} \theta(-\epsilon), \tag{57}$$

whereas $\Delta(\epsilon)$ is obtained from $\gamma(\epsilon)$ via a subtracted dispersion relation. We follow Ref. [32,33] in setting $\alpha = 10.75$ MeV, $\epsilon_0 = 18$ MeV and $\epsilon_1 = 110$ MeV. The spectral

function is proportional to the imaginary part of the hole propagator, $S_{HM}^{(SW)} = \text{Im}G_{HM}^{(SW)}/\pi$: Hence, in principle, the spreading width extends the support of the spectral function to the whole first quadrant of the (\mathcal{E}, p) plane; in practice, $S_{HM}^{(SW)}$ remains concentrated around the lines where the spectral function for a pure harmonic oscillator is non-vanishing.

We turn now to an examination of some of the model dependences that we obtain. In Figs. 6 and 7, we display the neutrino cross sections for the HM and its extended version with a spreading width for the same kinematical conditions explored above using the RFG. One sees from the figures that, although the basic features of the RFG cross sections studied in Section IV do not appear to be much altered by the nucleons' confinement, yet some differences do show up. In particular, the peaks of the cross sections in the HM appear shifted and the phenomenon of the vanishing of the cross section, which is characteristic of the RFG, is still present in the hybrid model, although in a narrower range of energies. Note also in comparing panels b) and c) that the effect of the spreading width, and therefore this particular class of correlation effects, is negligible and is henceforth ignored.

While the nuclear modeling used in these comparisons of RFG and HM results can obviously be extended in many directions, including the use of alternative mean-field bound wave functions and incorporation of final-state interaction effects, the theoretical uncertainties are likely reasonably characterized by the present "extreme" situations. Each model has its own merits. In particular, the RFG maintains covariance, which becomes more relevant for the BNL kinematics, whereas the HM brings in the confinement of the (off-shell) struck nucleon, albeit at the expense of covariance. Since the former involves only plane-wave nucleons while the latter has rather strongly confined HO wave functions for the struck nucleons, most other choices might be expected to fall somewhere between the results presented here. If the span of predictions given in the figures for the double-differential cross section is taken at face value, then substantial nuclear model dependences are anticipated and any hope of using absolute cross sections for the purpose of learning about axial-vector strangeness in the nucleon is correspondingly low. As we discuss in the next section, however, there does appear to be a strategy whereby one can mitigate this model-dependence in the extraction of Δs from neutrino observables.

VI. STRANGE AXIAL-VECTOR FORM FACTOR

We now address the use of neutrino scattering to probing nucleon strangeness. To this end, we recall that the nucleon's NC axial-vector form factor may be written as [1,28] (see the Appendix)

$$\tilde{G}_A = \left[\xi_A^{T=1} G_A^{(3)} \tau_3 + \xi_A^{T=0} G_A^{(8)} + \xi_A^{(0)} G_A^{(s)} \right] , \quad (58)$$

where

$$G_A^{(3)} = (1/2)(D + F)G_D^A(\tau) \quad (59a)$$

$$G_A^{(8)} = (1/2\sqrt{3})(3F - D)G_D^A(\tau) \quad (59b)$$

$$G_A^{(s)} = g_A^{(s)}G_D^A(\tau) \quad (59c)$$

$$D + F = 1.257 \quad (59d)$$

are SU(3) octet axial-vector form factors, D and F are the associated SU(3) reduced matrix elements, $g_A^{(s)} \equiv \Delta s$ is the strange quark contribution to the nucleon's axial charge, and $\tau = |Q|^2/4m_N^2$. The coefficients $\xi_A^{(a)}$ are determined by the axial-vector coupling of the Z^0 to the quarks, and take on, at tree level in the Standard Model, the values -2 , 0 , and 1 for a being $T = 1$, $T = 0$, and 0 , respectively. For neutrino scattering, electroweak radiative corrections are of $\mathcal{O}(\alpha/4\pi)$ [29,30], so for purposes of this analysis, we may employ the tree-level values. Under this approximation, any isoscalar component of the nucleon's axial-vector form factor arises solely from the strange quark term.

The quantity $G_D^A(\tau)$ is a dipole parameterization for the Q^2 -dependence of the axial-vector form factors. In principle, one has no rigorous justification for choosing a dipole form and for assuming that the different form factors in Eq. (59) display the same Q^2 -behavior. In the case of high-energy neutrino scattering, where values for $|Q^2|$ on the order of one $(\text{GeV}/c)^2$ are achieved, these assumptions can have rather drastic consequences for one's determination of Δs . As indicated in Refs. [2,3], the value of Δs is strongly correlated with the dipole mass parameter, M_A . As far as a high-energy neutrino scattering determination of Δs is concerned, the impact of choosing a different parameterization or of allowing the octet and singlet form factors to display different Q^2 -behavior is unknown. At kinematics relevant to the LSND experiment, the issue of non-leading Q^2 -dependence is much less serious. In this case, one may view the dipole form factors as a way to include the first derivative-term in a Taylor expansion of the form factor (with respect to Q^2). Moreover, as shown in Refs. [1,4], the correlation between Δs and M_A is negligible. Thus, we may safely employ the dipole parameterization for purposes of analyzing low-energy scattering without introducing significant uncertainty.

To illustrate the relationship between Δs and the choice of nuclear model, we first plot in Fig. 8 the differential cross section as a function of outgoing nucleon kinetic energy for two different values of Δs : 0 and -0.2 . The latter value corresponds roughly to the largest value (in magnitude) of Δs derived from the deep inelastic measurements. The results for kinematics typical of the LSND experiment are shown in Figs. 8a,b while those typical of the BNL measurements are given in Fig. 8c. We note that in the case of the LSND experiment, for which the target is a CH_2 based scintillator and for which the incident neutrinos are produced by the decay of pions in flight, a cut on T_N of > 60 MeV guarantees that only nucleons knocked out of carbon nuclei are detected [12]. For these energies, one sees from Figs. 8a,b that the nuclear model-dependence is sufficiently large to prevent an unambiguous extraction of Δs . For example, in the case of the proton knockout cross section, the difference between the RFG prediction for $\Delta s = 0$ and the HM prediction for $\Delta s = -0.2$ is comparable to or smaller than the difference between the RFG predictions with $\Delta s = 0$ and $\Delta s = -0.2$. This feature does not appear to persist at higher-energies (Fig. 8c) where the model-dependence for a given value of Δs is significantly smaller than the dependence on the value of Δs .

The authors of Ref. [12] proposed that instead of analyzing the proton and neutron cross sections separately, one ought to consider the *ratio* of total proton to neutron yields. In contrast to the situation with the individual cross sections, the yield ratio is insensitive to one of the primary experimental uncertainties – the normalization of the incident neutrino flux. Moreover, it was shown in Ref. [13] that the yield ratio is less sensitive to final-

state interactions than are the individual cross sections. Thus, the use of the p/n ratio would appear to minimize the impact of experimental and theoretical uncertainties on the extraction of Δs from QE neutrino scattering data. In what follows, we illustrate the degree to which the use of this ratio can also reduce one's sensitivity to the choice of nuclear model. We work with the ratio of cross sections rather than yields, assuming as in Ref. [12] that the incident fluxes are peaked at some energy $\bar{\epsilon}$ and that working with the cross sections at $\epsilon = \bar{\epsilon}$ is sufficient. To that end, we first show in Fig. 9 the ratio of differential proton knockout and neutron knockout cross sections as a function of T_N . From these curves, we deduce that the spread due to the choice of nuclear model for a given value of Δs and T_N is roughly 20% or less than the change in the ratio obtained by varying Δs from zero to -0.2 .

In Fig. 10 we give the total cross sections, integrated over outgoing nucleon energy (with $T_N > 60$ MeV in the case of low-energy neutrinos and $T_N > 200$ MeV for high-energy neutrinos) as functions of Δs . In the case of the LSND experiment, it is the total proton and neutron yields that will be obtained, making these curves more directly relevant to the interpretation of the experiment. From Fig. 10a,b, one sees that the model-sensitivity of one's extracted value of Δs is non-trivial in the case of low-energy neutrino scattering. For a given value of the total cross section, the two would yield values of Δs differing by about 0.5. Thus, we would take a reasonable nuclear theory error bar on the value of Δs extracted from the single cross section to be $\delta_{\text{nuc}}(\Delta s) = \pm 0.25$. This uncertainty is as large in magnitude as the value of Δs determined from deep inelastic scattering. For higher energy scattering, however, the corresponding nuclear model uncertainty is much smaller: $\delta_{\text{nuc}}(\Delta s) = \pm 0.015$ (see Fig. 10c).

Finally, in Fig. 11 we give the ratio R_ν of proton to neutron total cross sections for low-energy scattering. In this case, one finds that the ratio is significantly less sensitive to the choice of nuclear model than in the case of the actual cross sections themselves. Indeed, we would deduce a nuclear theory uncertainty in Δs of $\approx \pm 0.015$ from the curves in Fig. 11. This uncertainty represents an order of magnitude improvement from the uncertainty associated with the use of the individual cross sections.

One other issue involving model dependence was also briefly examined, namely, that of the on- versus off-shell current descriptions employed. We evaluated the HM results using the on-shell single-nucleon current and found that R_ν in that case is lower than the RFG curve by about the amount it is higher for the off-shell results shown in Fig. 11. Of course, such a calculation is not strictly correct and should be used only as a rough indication of the sensitivity to the prescription for the current, since some off-shellness must be used for the HM as demanded by the kinematics of the reaction. In fact, the rather weak dependence found is reassuring and suggests that, at least for the specific kinematical choices that are relevant here, the issue of what particular single-nucleon current to employ is likely even less important than the nuclear model dependence. To be as conservative as possible, we will multiply by two the uncertainty deduced from Fig. 11 and take $\delta_{\text{nuc}}(\Delta s) = \pm 0.03$.

The reason for this reduction in nuclear model sensitivity when using R_ν is straightforward to understand. At the kinematics typical of the LSND experiment, the range of Q^2 accessed as one integrates over the allowed region $\mathcal{D}(\theta_N)$ is small. Consequently, the nucleon form factors and kinematic factors vary gently and, to a first approximation, may be factored out of the integral in the expression of Eq. (35). One is then left with a product of the squared single-nucleon invariant amplitude and an integral of the one-body spectral func-

tion. Differences between model predictions would then arise from different distributions of strength in the spectral function over the allowed domain in the (\mathcal{E}, p) plane. In the ratio of proton and neutron cross sections, the integrals of the spectral functions should cancel assuming the proton and neutron $S(p, \mathcal{E})$ are identical. In this case, the ratio is independent of nuclear model and is determined only by the single-nucleon form factors. Any model dependence which appears in the ratio would then arise from one of the following sources: (i) the variation in form factors and kinematic factors over the integration region $\mathcal{D}(\theta_N)$, so that the factorization into a product of single-nucleon and many-body physics is not exact; (ii) differences between proton and neutron spectral functions; (iii) contributions going beyond the PWIA. In the case of low-energy neutrino scattering from carbon for $T_N > 60$ MeV, one expects the effects (i) and (ii) to be small. Indeed, our results indicate that effects of type (i) generate roughly a 10% variation in the ratio for a given value of Δs , which translates into the nuclear theory uncertainty quoted above.

In arriving at our estimate of the nuclear theory uncertainty, we make no pretense of having performed definitive, state-of-the-art nuclear model calculations of the kind reported in Refs. [12,13]. Rather, our goal was to give a reasonable upper bound on the expected spread in model calculations. We anticipate that any series of more sophisticated model calculations would yield extractions of Δs from R_ν differing by no more than our value for $\delta_{\text{nuc}}(\Delta s)$. From this standpoint, it is instructive to compare our RFG and HM results for this ratio with the mean field calculation reported in Ref. [12]. For a given value of Δs , the mean field results and RFG results for R_ν are almost identical, while the HM results differ by less than 10%. This agreement holds in spite of much larger differences which appear when one compares the mean field, RFG, and HM predictions for the individual differential cross sections and for the ratio of differential cross sections as a function of T_N . We further believe that this robust nature of R_ν will persist when one compares different model calculations which not only reproduce experimental results for the inclusive t -channel QE responses but also include FSI's in the u -channel case. It was demonstrated in Ref. [13] that the inclusion of FSI's in the mean field approach can increase the predicted value of R_ν by more than 10% over the mean field and RFG predictions. This increase would imply a shift in the extracted value of Δs by more than 0.03. Thus, it appears that any realistic model which is used in this extraction must include FSI's. Nevertheless, we would argue that the *spread* in extracted values of Δs corresponding to the use of different nuclear models which include FSI's would remain smaller than $\delta_{\text{nuc}}(\Delta s)$. Indeed, an important check on our first estimate of $\delta_{\text{nuc}}(\Delta s)$ would be to compare model calculations which incorporate FSI's as well as to explore the impacts of correlations and charge symmetry breaking.

Finally, we compare the nuclear theory uncertainty in the neutrino scattering determination of Δs with the theory uncertainties associated with the extraction of Δs from measurements of the $g_1(x, Q^2)$ deep inelastic structure function. We first remind the reader that one does not necessarily expect the values of Δs obtained from these two different processes to agree. It has long been known, but perhaps not widely appreciated in the nuclear physics community, that Δs is a renormalization-scale dependent quantity. In deep inelastic scattering, this scale is typically taken to be the same as the mean $\sqrt{|Q^2|}$ of the reaction (between $\sqrt{2}$ and $\sqrt{11}$ GeV/ c), whereas the scale appropriate to the quasielastic neutrino value is somewhere below the charm quark mass. The latter corresponds to the scale below

which one includes only the three lightest quarks in an effective axial-vector NC [34]. It is often assumed that the QCD evolution of Δs between the two scales is rather gentle, based on leading-order perturbative calculations, yet it is conceivable that non-perturbative effects could invalidate this assumption [35]. At present, one can make no definitive statements regarding the evolution of Δs between these two scales.

A separate issue pertaining to the use of polarized structure functions to determine Δs is the use of SU(3) symmetry. In the standard operator product analysis of the g_1 -sum, one employs an SU(3) parameterization of the octet axial-vector matrix elements $\langle N|A_\mu^{(a)}(0)|N\rangle$ ($a = 3, 8$ refers to the respective components of the octet) in order to derive a value for Δs or $\Delta\Sigma$. The latter denotes the nucleon's singlet axial charge or, in the quark-parton framework, the total light quark (u, d, s) contribution to the nucleon spin. The value of Δs determined in this fashion is quite sensitive to the quantity

$$\frac{2}{\sqrt{3}}\langle N|A_\mu^{(8)}(0)|N\rangle = \frac{1}{3}(3F - D) \quad . \quad (60)$$

In an SU(3)-symmetric fit to hyperon semileptonic decays, the combination of reduced matrix elements $3F - D$ takes on a value of about 0.6 [23]. Because it involves a cancellation between two quantities, this number is rather sensitive to uncertainties in the fit as well as to corrections arising from SU(3)-breaking in the octet matrix elements. Several analyses have been carried out recently [22,23,36,37] in which the hyperon decays were re-fit with allowance for SU(3)-breaking. While different schemes for the incorporation of SU(3)-breaking were employed in each case, a general trend does emerge: SU(3)-breaking may reduce the matrix element in Eq. (60) by 50% or more compared to its SU(3)-symmetric value, with an uncertainty of comparable magnitude. Such a reduction would imply a value of $\Delta s \approx 0$ from deep inelastic data, in contrast to the current average of the measurements $\Delta s \approx -0.1$. The authors of these studies caution that precise numerical value for the SU(3)-breaking correction to the quantity in Eq. (60) is not highly reliable, due to the nature of the aforementioned cancellation. To be conservative, then, we take the SU(3)-breaking uncertainty in this matrix element to be 50% of its SU(3)-symmetric value. The corresponding uncertainty in the strange-quark axial charge is $\delta_{\text{DIS}}(\Delta s) \approx \pm 0.1$, a value having the same magnitude as the present average for Δs under the assumption of good SU(3) symmetry in the hyperon semi-leptonic decays. The scale of this uncertainty is consistent with the scale of the error obtained with the heavy-baryon chiral perturbation theory analysis of Ref. [22] and with the range of estimates for SU(3)-breaking corrections given in Refs. [23,36,37]. The presence of this SU(3)-uncertainty weakens the standard conclusion drawn from inclusive, polarized deep inelastic measurements that the strange quarks are polarized oppositely to the direction of the nucleon's spin and that the magnitude of the $s\bar{s}$ contribution is about one-third the total quark contribution, $\Delta\Sigma$.

By way of comparison, we note that $\delta_{\text{nuc}}(\Delta s)$ is about one-third as large as $\delta_{\text{DIS}}(\Delta s)$. Moreover, the analysis of the QE neutrino cross sections does not suffer from the kind of SU(3)-breaking corrections and uncertainties which enter the interpretation of the g_1 -sum results. Although the same problematic combination of SU(3) reduced matrix elements $3F - D$ enters the decomposition of the nucleon's axial-vector NC form factor (see Eqs. 58-59), its contribution is suppressed by the coupling $\xi_A^{T=0}$. The latter is identically zero at tree level in the Standard Model and is on the order of 0.01 when one-loop electroweak

corrections are included. From this standpoint, then, it appears that the ratio R_ν provides a theoretically cleaner window on the strange-quark contribution to the nucleon's spin than does inclusive, polarized deep inelastic scattering. The primary limitation in the former case appears to be experimental error.

VII. CONCLUSIONS

The study of low- and intermediate-energy semi-leptonic processes has played an important role in helping uncover the nature of fundamental interactions. In the case of QCD, semi-leptonic scattering is poised to illuminate the way the strong interaction is realized in the structure of the nucleon. As with the use of semi-leptonic scattering to test the Standard Model and its possible extensions, the efficacy of this probe of the nucleon's structure is limited by the reliability with which one can compute theoretically, or determine experimentally, the other hadron and nuclear structure contributions to the relevant observables. It is important, then, that where hadron structure or many-body theory is brought to bear on the interpretation of such observables, an attempt be made to quantify the theoretical uncertainty.

In the present work, we have attempted to provide a theoretical error bar for the determination of Δs from quasielastic neutrino NC scattering. The nucleon's strange quark axial charge is of interest since it has the quark-parton interpretation as giving the strange-quark contribution to the spin of a polarized nucleon. A large value for this quantity would imply that the non-valence quarks play a more central role in the low-energy characteristics of the nucleon than implied by the highly-successful and intuitively satisfying quark model. To the extent that one may extract the nucleon's NC axial-vector form factor from quasielastic neutrino scattering at low momentum transfer, one has a direct probe of Δs . In the ideal situation, one would have in hand sufficient information from quasielastic $(e, e'N)$ measurements to perform this extraction without heavy reliance on theoretical calculations of the QE response. At present, sufficient $(e, e'N)$ data are lacking, rendering the use of nuclear models unavoidable.

We have tried to argue that were one to rely on the individual $(\nu, N)\nu'$ cross sections measured by LSND, the nuclear theory error bar on Δs would be sufficiently large to render the results inconclusive. Fortunately, the ratio of total proton to neutron yields (R_ν) appears to be much less sensitive to the choice of nuclear model, reducing by nearly one order of magnitude the nuclear theory uncertainty in Δs . Based on the study of some simple nuclear models with quite distinct assumptions regarding the many-body dynamics, we estimate the nuclear theory error to be $\delta_{\text{nuc}}(\Delta s) = \pm 0.03$. We anticipate that the spread in values for Δs obtained from R_ν and more sophisticated nuclear models will be smaller than this value for the uncertainty. We further note that $\delta_{\text{nuc}}(\Delta s)$ is about a factor of three smaller in magnitude than $\delta_{\text{DIS}}(\Delta s)$, where the latter is derived from recent analyses of SU(3)-breaking in the octet of baryon axial-vector matrix elements. In contrast, the interpretation of QE neutrino cross sections is relatively free from such SU(3)-uncertainties.

Acknowledgements: The authors from Torino would like to thank the INT in Seattle for the hospitality extended to them during one phase of the work on this project. We also

gratefully acknowledge useful discussions with A. Adelberger, M. Frank, W. Haxton, and C. Johnson.

APPENDIX:

The quantities appearing in Eq. (51) are given by the following expressions:

$$V_{VV} = 2[V_{11} + V_{12} + V_{22}] \quad (\text{A1})$$

$$V_{VA} = 2[V_{A1} + V_{A2}] \quad (\text{A2})$$

$$V_{AA} = 2A \quad (\text{A3})$$

using the nomenclature of Ref. [4]. On-shell one has from that reference

$$V_{11} = 4\tilde{F}_1^2(P \cdot K P_N \cdot K' + P_N \cdot K P \cdot K' - m_N^2 K \cdot K') \quad (\text{A4})$$

$$V_{12} = -4\tilde{F}_1\tilde{F}_2 K \cdot K' (P_N - P) \cdot (K - K') \quad (\text{A5})$$

$$V_{22} = \frac{2\tilde{F}_2^2}{m_N^2} K \cdot K' (P \cdot K P_N \cdot K + P \cdot K' P_N \cdot K' + m_N^2 K \cdot K') \quad (\text{A6})$$

$$A = 4\tilde{G}_A^2(P \cdot K P_N \cdot K' + P_N \cdot K P \cdot K' + m_N^2 K \cdot K') \quad (\text{A7})$$

$$V_{A1} = 8\tilde{G}_A\tilde{F}_1(P \cdot K P_N \cdot K' - P_N \cdot K P \cdot K') \quad (\text{A8})$$

$$V_{A2} = 4\tilde{G}_A\tilde{F}_2 K \cdot K' (P + P_N) \cdot (K + K') , \quad (\text{A9})$$

where P and P_N are the initial and final four-momenta of the nucleon, K and K' the initial and final four-momenta of the neutrino, \tilde{G}_A is the axial-vector form factor of the nucleon whereas \tilde{F}_1 and \tilde{F}_2 are the Dirac and Pauli weak NC form factors of the nucleon, related to the Sachs NC form factors through the expressions $\tilde{G}_E = \tilde{F}_1 - \tau\tilde{F}_2$ and $\tilde{G}_M = \tilde{F}_1 + \tilde{F}_2$, with $\tau = |Q^2|/4m_N^2$. For the nucleon's form factors we have used the Galster parameterization (see Refs. [28,31]). These can be combined as in Eqs. (A1–A3) to obtain the following for the on-shell versions of the quantities in Eq. (51):

$$V_{VV}^{on} = m_N^4 \left\{ \left(\frac{Y \cdot Z}{m_N^2} \right)^2 \tilde{W}_2 - 16\tau(\tilde{G}_E^2 - \tau\tilde{G}_M^2) \right\} \quad (\text{A10})$$

$$V_{VA}^{on} = m_N^4 \left\{ 16 \left(\frac{Y \cdot Z}{m_N^2} \right) \tau\tilde{G}_M\tilde{G}_A \right\} \quad (\text{A11})$$

$$V_{AA}^{on} = m_N^4 \left\{ \left[\left(\frac{Y \cdot Z}{m_N^2} \right)^2 + 16\tau(1 + \tau) \right] \tilde{G}_A^2 \right\} . \quad (\text{A12})$$

Here we have used the following four-vectors: $Q = K - K' = P_N - P$, $Y \equiv K + K'$ and $Z \equiv P_N + P$, where then $Q \cdot Y = 0$ and for on-shell nucleons $Q \cdot Z = 0$. Furthermore, we define as usual $\tilde{W}_2 \equiv [\tilde{G}_E^2 + \tau \tilde{G}_M^2]/(1 + \tau)$.

Off-shell we use a generalization of the *cc1* prescription introduced by de Forest [25] for electron scattering; in our case we now have analogous quantities involving both vector and axial-vector neutral currents. Defining, as usual, $P^\mu \equiv P_N^\mu - Q^\mu = (E, \mathbf{p})$, letting $\bar{P}^\mu \equiv P_N^\mu - \bar{Q}^\mu = (\bar{E}, \mathbf{p})$, with $\bar{E} \equiv \sqrt{m_N^2 + p^2}$ as in Ref. [25], and in addition defining $\bar{Z}^\mu \equiv P_N^\mu + \bar{P}^\mu$, so that $Q \cdot Y = \bar{Q} \cdot \bar{Z} = 0$, we obtain

$$V_{VV}^{off} = \left[(Q \cdot \bar{Q})^2 - (\bar{Q} \cdot Y)^2 \right] \tilde{G}_M^2 + 4m_N^2 Q^2 \tilde{G}_E'^2 + \left[(Y \cdot \bar{Z})^2 - (Q \cdot \bar{Z})^2 \right] \tilde{W}_2' \quad (\text{A13})$$

$$V_{VA}^{off} = 4 \left[(Q \cdot \bar{Z}) (\bar{Q} \cdot Y) - (Q \cdot \bar{Q}) (Y \cdot \bar{Z}) \right] \tilde{G}_M \tilde{G}_A \quad (\text{A14})$$

$$V_{AA}^{off} = \left[(Q \cdot \bar{Q})^2 + (Y \cdot \bar{Z})^2 - (Q \cdot \bar{Z})^2 - (\bar{Q} \cdot Y)^2 - 4m_N^2 Q^2 \right] \tilde{G}_A^2. \quad (\text{A15})$$

In Eq. (A13) we have introduced the following additional single-nucleon form factors:

$$\tilde{G}_E' \equiv \tilde{F}_1 - \bar{\tau} \tilde{F}_2 \quad (\text{A16})$$

$$\tilde{W}_2' \equiv \frac{1}{1 + \bar{\tau}} \left[\tilde{G}_E'^2 + \bar{\tau} \tilde{G}_M^2 \right] \quad (\text{A17})$$

in close analogy with the above on-shell quantities (see also Ref. [38]). The results given here for the half-off-shell currents revert to the on-shell results in Eqs. (A10–A12) when P and \bar{P} become the same, *i.e.*, when the kinematics force the nucleon on-shell.

REFERENCES

- [1] M. J. Musolf, T. W. Donnelly, S. J. Pollock, S. Kowalski, and E. J. Beise, Phys. Rep. **239**, 1 (1994).
- [2] L. A. Ahrens *et al.*, Phys. Rev. **D35**, 785 (1987).
- [3] G. T. Garvey, W. C. Louis, and D. H. White, Phys. Rev. **C48**, 761 (1993).
- [4] C. J. Horowitz, H. Kim, D. P. Murdock, and S. Pollock, Phys. Rev. **C48**, 3078 (1993).
- [5] J. A. Ashman *et al.* (EMC collaboration), Nucl. Phys. **B328**, 1 (1989).
- [6] B. Adeva *et al.* (SMC collaboration), Phys. Lett. **B302**, 533 (1993).
- [7] P. L. Anthony *et al.* (E142 collaboration), Phys. Rev. Lett. **71**, 959 (1993).
- [8] B. Adams *et al.* (SMC collaboration), Phys. Lett. **B329**, 399 (1994).
- [9] K. Abe *et al.* (E143 collaboration), Phys. Rev. Lett. **74**, 346 (1995).
- [10] These analyses indicate a strong correlation between Δs and M_A , the dipole mass parameter appearing in standard parameterizations of the axial-vector form factor. In Ref. [3], a fit performed forcing $\Delta s = 0$ yields a value of M_A higher than the world average. The other three fits, in which Δs is allowed to vary, yield smaller $\chi^2/\text{D.O.F.}$ and values for M_A consistent with the 1987 world average.
- [11] LSND Collaboration, Los Alamos Proposal No. 1173, W. C. Louis, contact person (unpublished).
- [12] G. T. Garvey, S. Krewald, E. Kolbe, and K. Langanke, Phys. Lett. **B289**, 249 (1992).
- [13] G. T. Garvey, E. Kolbe, K. Langanke, and S. Krewald, Phys. Rev. **C48**, 1919 (1993).
- [14] MIT-Bates Proposal No. 89-06, R. D. McKeown and D. H. Beck, spokespersons (unpublished).
- [15] MIT-Bates Proposal No. 94-11, M. Pitt and E. J. Beise, spokespersons (unpublished).
- [16] CEBAF Proposal No. PR-91-004, E. J. Beise, spokesperson (unpublished).
- [17] CEBAF Proposal No. PR-91-017, D. H. Beck, spokesperson (unpublished).
- [18] CEBAF Proposal No. PR-91-010, J. M. Finn and P. A. Souder, spokespersons (unpublished).
- [19] Mainz Proposal A4/1-93, E. Heinen-Konschak *et al.*, collaborators, D. von Harrach, spokesperson.
- [20] R. Cenni, T. W. Donnelly and A. Molinari, (to be published).
- [21] J. Jourdan, Phys. Lett. **B353**, 189 (1995); see also T. C. Yates, *et al.*, Phys. Lett. **B312**, 382 (1993).
- [22] E. Jenkins and A. Manohar, Phys. Lett. **B255**, 558 (1991).
- [23] J. Dai, R. Dashen, E. Jenkins, A. V. Manohar, UCSD Preprint PTH 94-19 (1995).
- [24] D. B. Day, J. S. McCarthy, T. W. Donnelly and I. Sick, Ann. Rev. Nucl. Part. Sci. **40**, 357 (1990).
- [25] T. de Forest, Nucl. Phys. **A392**, 232 (1983).
- [26] J. D. Bjorken and S. D. Drell, *Relativistic Quantum Mechanics* (McGraw-Hill, New York, 1964).
- [27] W. M. Alberico, A. Molinari, T. W. Donnelly, E. L. Kronenberg and J. W. Van Orden, Phys. Rev. **C47**, 1801 (1988).
- [28] M. J. Musolf and T. W. Donnelly, Nucl. Phys. **A546**, 509 (1992); 550 (1992) 564(E).
- [29] W. J. Marciano and A. Sirlin, Phys. Rev. **D22**, 2695, (1980).
- [30] M. J. Musolf and B. R. Holstein, Phys. Lett. **B242**, 461 (1990).

- [31] T. W. Donnelly, M. J. Musolf, W. M. Alberico, M. B. Barbaro, A. De Pace and A. Molinari, Nucl. Phys. **A541**, 525 (1992).
- [32] C. Mahaux and H. Ngô, Phys. Lett. **100B**, 285 (1981).
- [33] R.D. Smith and J. Wambach, Phys. Rev. **C38**, 100 (1988).
- [34] D. Kaplan and A. Manohar, Nucl. Phys. **B310**, 527 (1988).
- [35] R. L. Jaffe and A. Manohar, Nucl. Phys. **B337**, 509 (1990).
- [36] B. Ehrensperger and A. Schafer, UFTP Preprint 377-1994 (1994).
- [37] J. Lichtenstadt and H. Lipkin, Tel Aviv Preprint TAUP-2244-95.
- [38] J. A. Caballero, T. W. Donnelly and G. I. Poulis, Nucl. Phys. **A555**, 709 (1993).

FIGURES

FIG. 1. Feynman diagram for exclusive lepton scattering in the one boson exchange approximation.

FIG. 2. The domain \mathcal{D} over which one integrates for the t -inclusive cross section at typical values of momentum and energy transfer. Note the more complex structure of the boundary when the intercept I_t given by Eq. 5 is positive.

FIG. 3. The same as Fig. 2 for the u -inclusive cross section: a) LSND kinematics ($\epsilon = 200$ MeV, $T_N = 60$ MeV); b) BNL kinematics ($\epsilon = 1.3$ GeV, $T_N = 60$ MeV). The boundaries shown all involve \mathcal{E}^- except for line BF which involves \mathcal{E}^+ . Note that when the neutrino and outgoing nucleon momenta are antiparallel quite remote regions of the (\mathcal{E}, p) plane are explored.

FIG. 4. Plane-wave impulse approximation version of the diagram in Fig. 1.

FIG. 5. Variation of the squared four-momentum transfer in the (\mathcal{E}, p) plane for the kinematical conditions of the LSND experiment. Note the rather mild dependence on \mathcal{E} and the strong dependence on p .

FIG. 6. The u -inclusive double differential cross section for protons (solid) and neutrons (dashed) for LSND kinematics and two different orientations of \mathbf{k} and \mathbf{p}_N : (a) RFG model, (b) HM with harmonic oscillator wave functions and (c) as for (b), but including a spreading width, or equivalently, a complex nucleon self-energy. Note the negligible effect of the last. Note also that, although we display the results over the whole allowed range of T_N , in the LSND experiment only nucleons with $T_N > 60$ MeV are actually detected.

FIG. 7. The same curves as in Fig. 6, but now for BNL kinematics. Note the double peak behaviour of the cross section at $\theta_N = 20^\circ$ (see text for discussion). Note also that, although we display the results over the whole allowed range of T_N , in the BNL experiment only nucleons with $T_N > 200$ MeV are actually detected.

FIG. 8. (a) The effect of axial-vector strangeness in the RFG and HM proton ejection cross sections for LSND kinematics integrated over angle for two values of $g_A^{(s)}$. Note the significant increase of the cross section induced by strangeness. (b) The same as (a), but now for neutrons. Note the significant reduction of the cross section induced by strangeness. (c) The same as (a), but now for BNL kinematics.

FIG. 9. Ratio between the angle-integrated cross sections for proton and neutron ejection at LSND kinematics. Both the RFG (dashed) and HM (solid) results are displayed.

FIG. 10. Total cross section (integrated over angle and energy) versus the strangeness content of the nucleon for outgoing protons (a) and neutrons (b) at LSND kinematics and (c) for protons at BNL kinematics. Dashed lines: RFG; solid: HM.

FIG. 11. The ratio of the proton and neutron total cross sections for LSND kinematics: Dashed line: RFG; solid: HM.

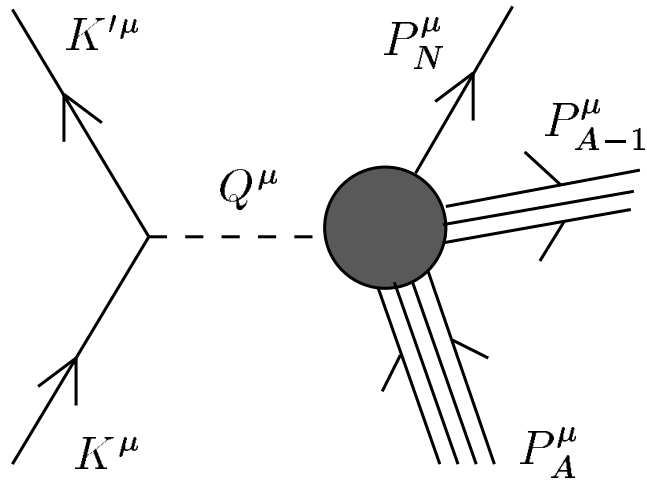


Fig. 1

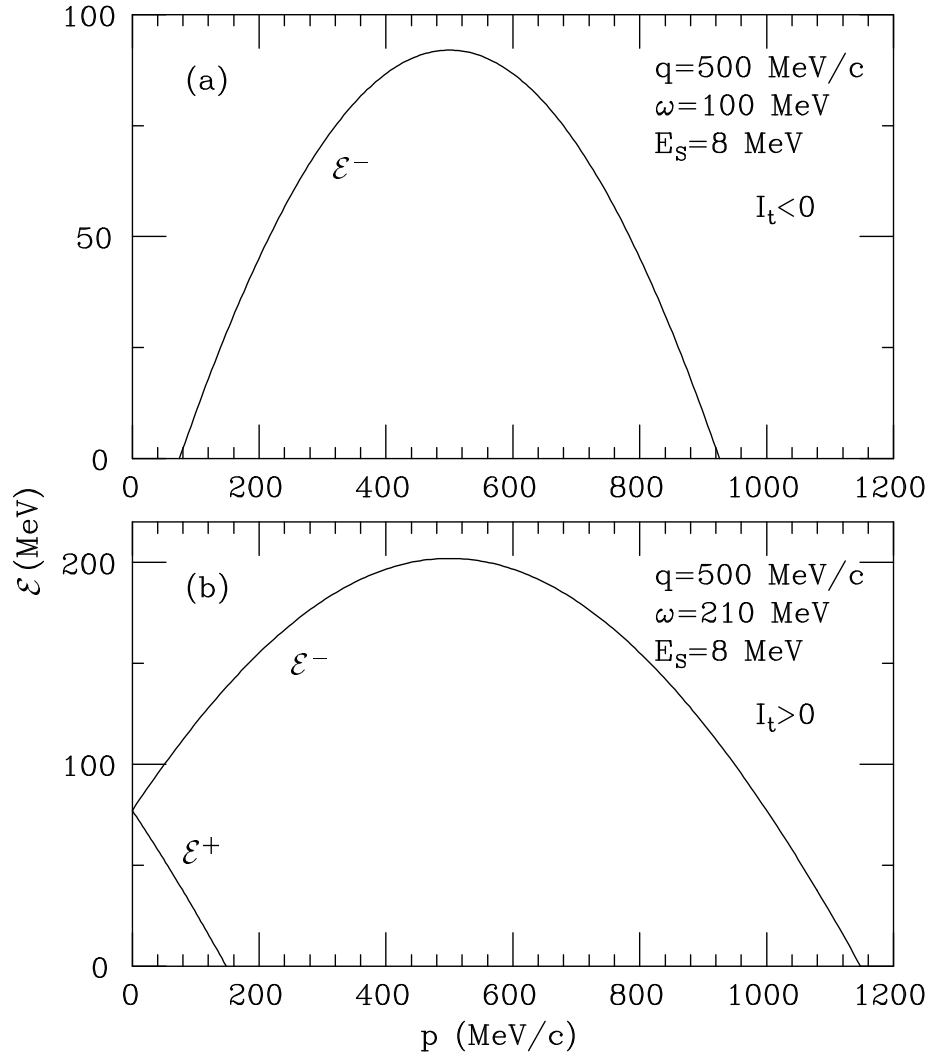


Fig. 2

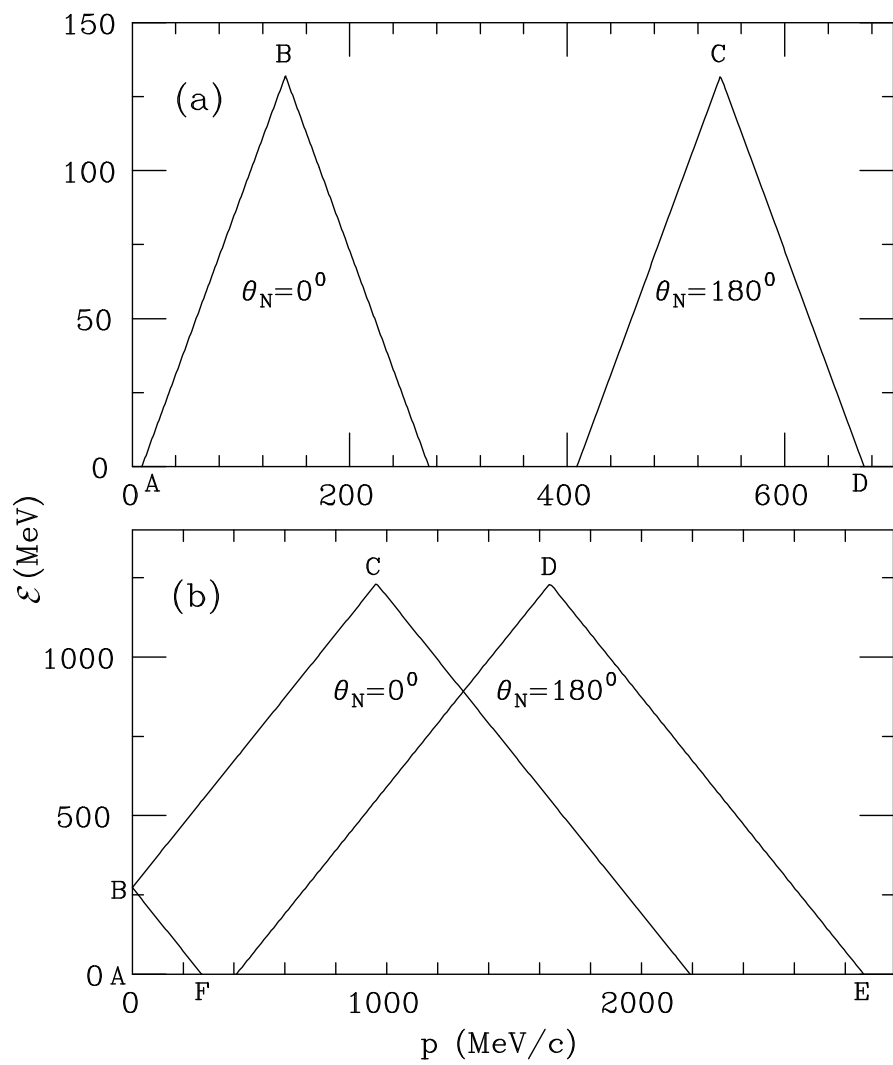


Fig. 3

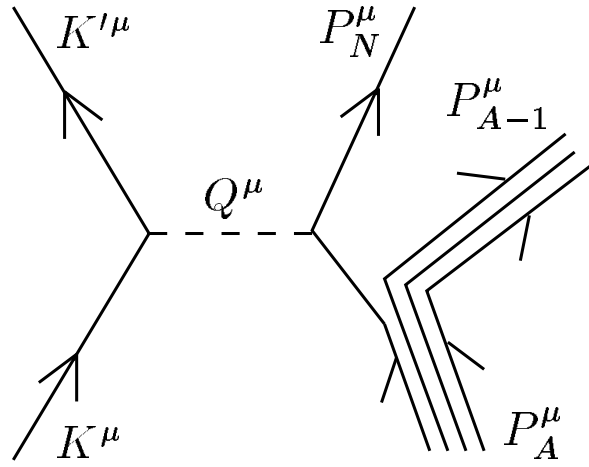


Fig. 4

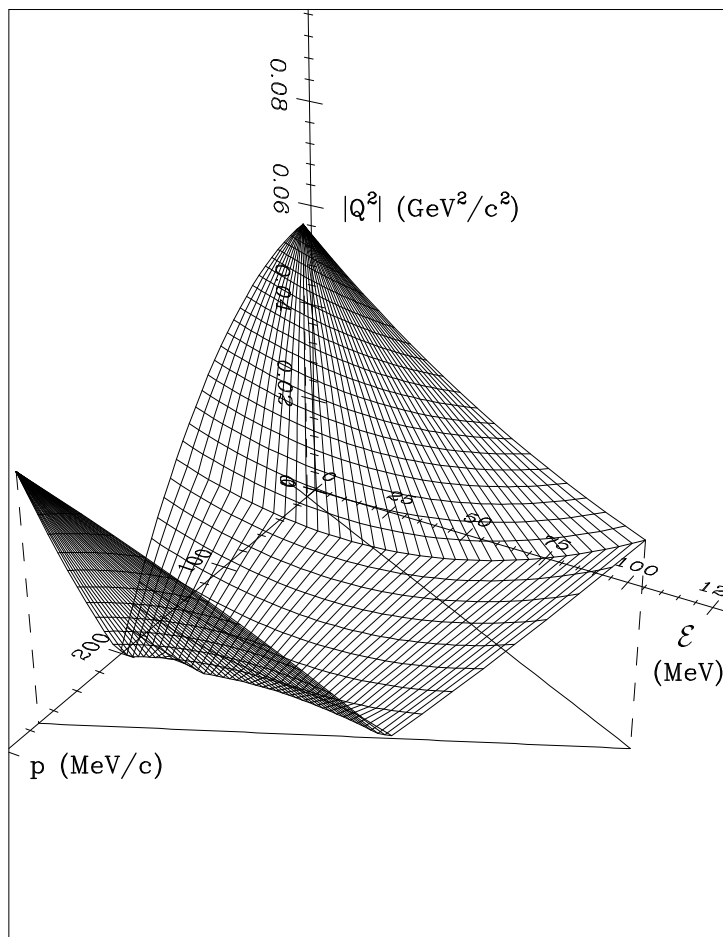


Fig. 5

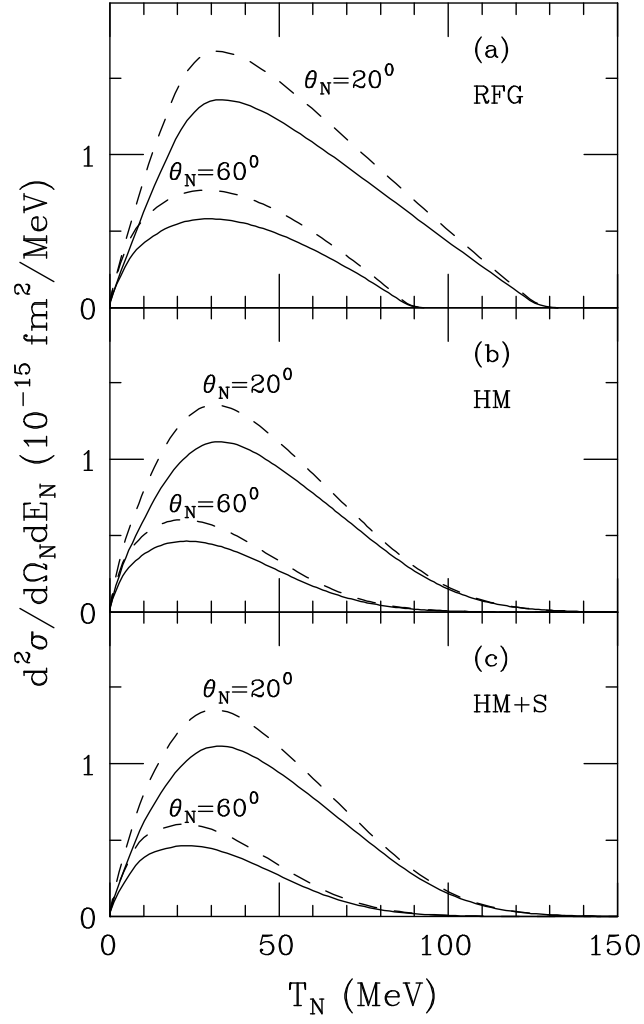


Fig. 6

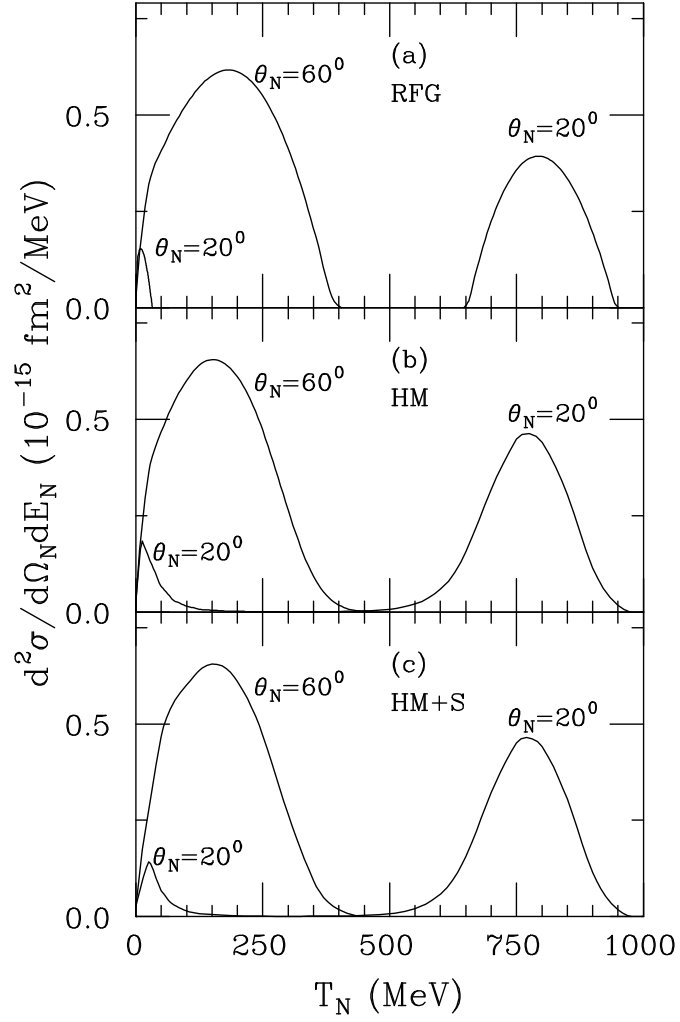


Fig. 7

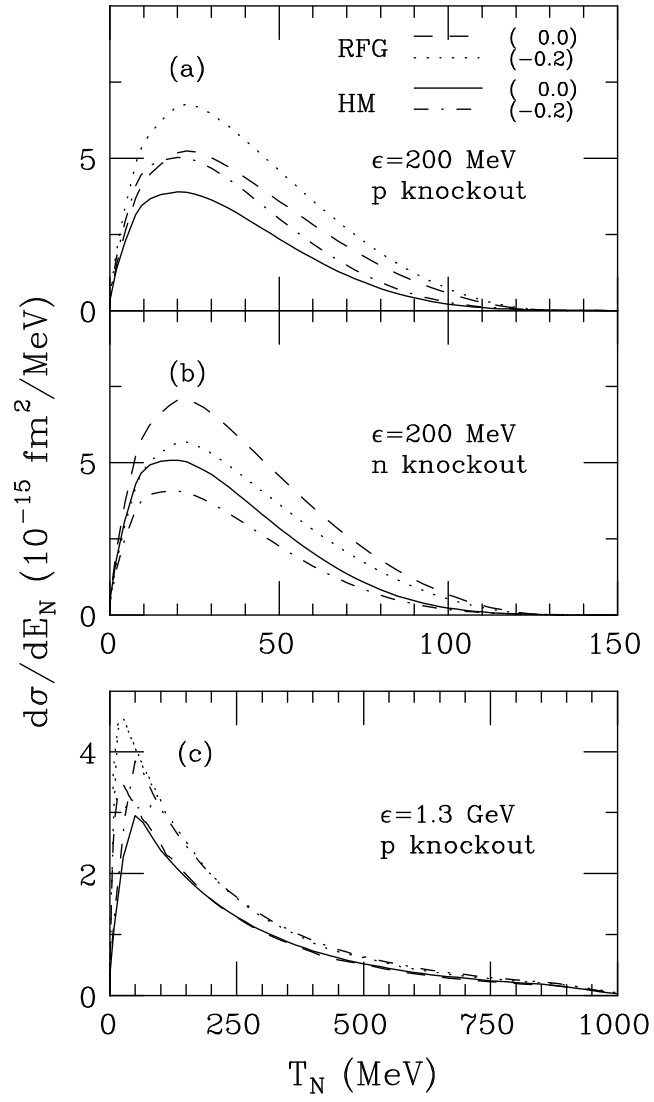


Fig. 8

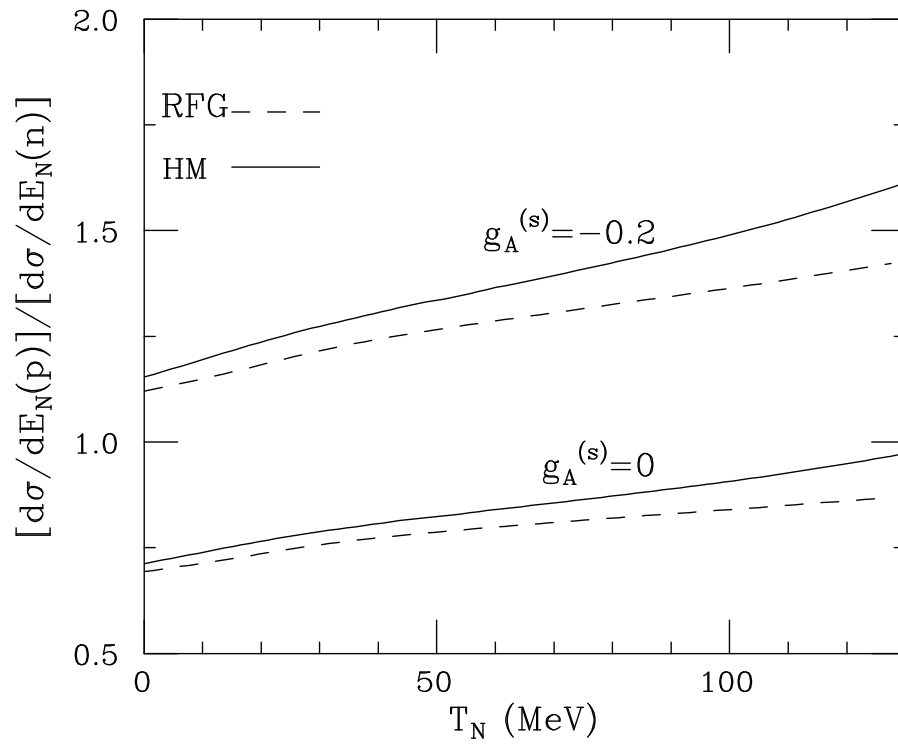


Fig. 9

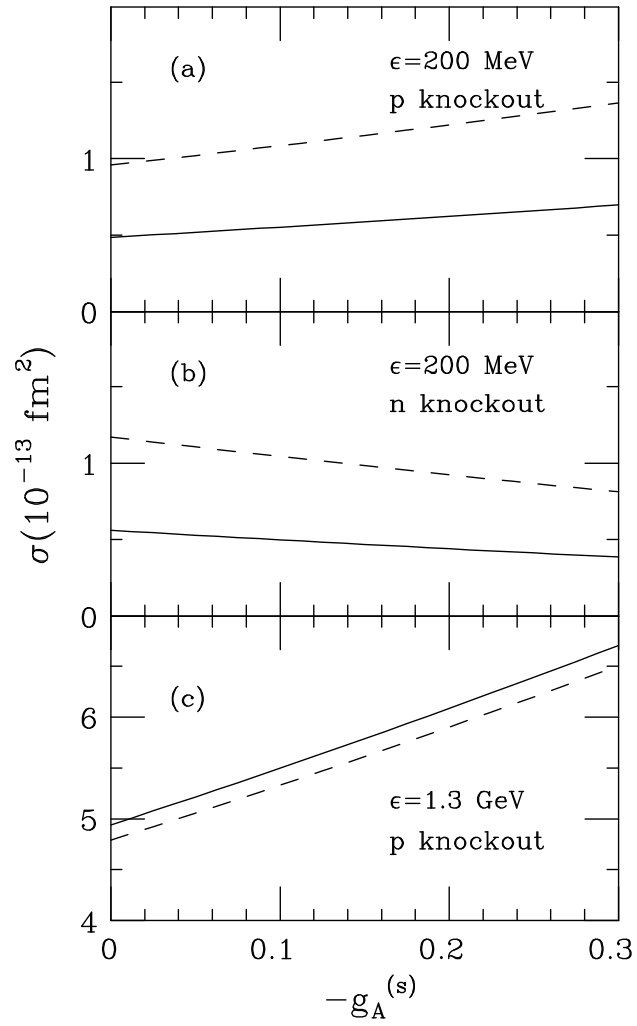


Fig. 10

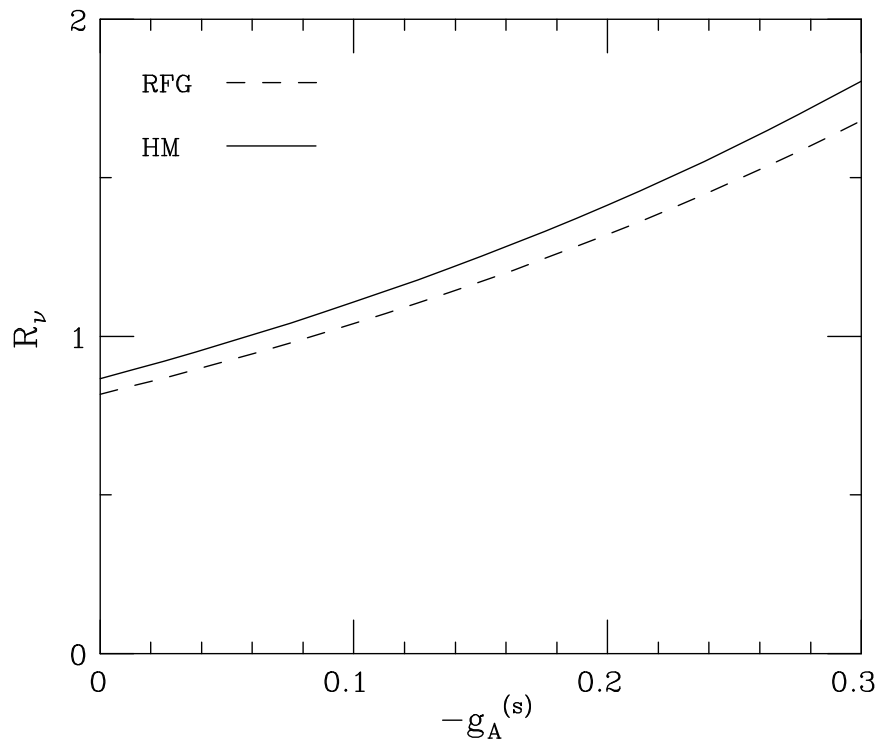


Fig. 11